UNIVERSIDAD DE CONCEPCIÓN
FACULTAD DE CIENCIAS FÍSICAS Y MATEMÁTICAS

VARIABILIDAD TEMPORAL DE LA ALTITUD DE LA ISOTERMA 0°C SOBRE LA ZONA COSTERA DEL BIOBIO (36.8°S), CHILE: CARACTERIZACIÓN Y ESTUDIO DE CASOS

Por: Camila Elizabeth Quijada Meza

Tesis presentada a la Facultad de Ciencias Física y Matemáticas de la Universidad de Concepción para optar al grado académico de Magíster en Geofísica

Diciembre 2024
Concepción, Chile

Profesor Guía: Dr. Martín Jacques Coper
Profesor Co-guía: Dr. René Garreaud Salazar

UNIVERSIDAD DE CONCEPCIÓN
FACULTAD DE CIENCIAS FÍSICAS Y MATEMÁTICAS

VARIABILIDAD TEMPORAL DE LA ALTITUD DE LA ISOTERMA 0°C SOBRE LA ZONA COSTERA DEL BIOBIO (36.8°S), CHILE: CARACTERIZACIÓN Y ESTUDIO DE CASOS

Por: Camila Elizabeth Quijada Meza

Tesis presentada a la Facultad de Ciencias Física y Matemáticas de la Universidad de Concepción para optar al grado académico de Magíster en Geofísica

Diciembre 2024
Concepción, Chile

Profesor Guía: Dr. Martín Jacques Coper
Profesor Co-guía: Dr. René Garreaud Salazar
Comisión evaluadora:
Dra. Simone Schauwecker - Dr. Andrés Sepúlveda -
Dr. Francisco Lang

Dedicado a mis padres y hermanas

AGRADECIMIENTOS

En este periodo de formación, he aprendido el valor de la perseverancia y de mantenerme enfocada, incluso frente a las dificultades. Quiero expresar mi más profundo agradecimiento a mis padres Germán y Silvia por su apoyo incondicional; ustedes han sido un pilar fundamental en mi vida, gracias a su guía y amor, soy la persona que soy hoy. A mi hermana Catalina, quien ha sido testigo de mi crecimiento tanto académico como personal, gracias por estar siempre a mi lado junto a nuestra pequeña hermana Yzabella.

Quiero agradecier a los amigos que Geofísica me regaló: Natalia, Carlos, Pía y Sebastián. A pesar que todo, hemos sabido reencontrarnos y mantener nuestra amistad. A mi amiga del alma Tamara: Eres, una parte esencial de mi vida; gracias por escucharme cuando nadie más podía hacerlo.

A mi pareja, Gustavo, quien estuvo en mis días más difíciles, especialmente cuando pensaba que no podía más con la tesis. Has sido un apoyo invaluable, y tus palabras de ánimo fueron fundamentales para seguir adelante. También quiero agradecer a Karly por alegrar mis días. Gracias por no dejar que me rinda.

Agradezo a los investigadores Drs. Simone Schauwecker y René Garreaud por sus valiosos comentarios y colaboración. Extiendo mi gratitud a mi profesor guía Dr. Martín Jacques por su paciencia y apoyo. Al Dr. R. Muñoz por facilitar los datos que dieron inicio a esta investigación. Gracias al Centro de Ciencias del Clima y la Resiliencia, ANID/FONDAP Gant 1523A0002 y ANID/FONDECYT Project 1211412 por el financiamiento que hizo posible este trabajo.

Quiero rendir un agradecimiento especial a quien formaba parte de la comisión de esta tesis. Aunque ya no está físicamente con nosotros, su apoyo, sabiduría y cercanía siempre serán recordados. Aldo, tu legado permanece en quienes tuvimos el privilegio de aprender de ti.

Por último, a todas aquellas personas que, de alguna u otra manera, colaboraron con este proyecto, ya sea desde el ámbito académico o brindándome apoyo emocional. A cada uno de ustedes, los recuerdo con gratitud. ¡Gracias totales!

Resumen

Analizamos aspectos de la variabilidad interanual, mensual, sinóptica y subdiaria de la altura de la isoterma de 0°C (H0), utilizando el reanálisis ERA5, observaciones y estimaciones, sobre la zona costera de la Región del Biobío, Chile (36.8°S, 73°W). Esta región carece de mediciones de H0 basadas en radiosondas, pero aquí utilizamos la observación horaria de H0 a bordo de aviones que despegan y aterrizan en el Aeropuerto Internacional Carriel Sur (SCIE, 36.77°S, 73.06°W) para el período 2017-2019. Validamos H0 del reanálisis usando observaciones, lo que revela un excelente rendimiento de ERA5. H0 varía a lo largo del año con un máximo en enero y un mínimo en julio. Luego, estimamos H0 en base a datos un Micro Rain Radar adquiridos en el Observatorio de Ríos Atmosféricos en Concepción para 2022 y 2023 con alta resolución vertical y temporal. En particular, usamos perfiles verticales de velocidad de caída y reflectividad de hidrometeoros durante eventos de precipitación. La velocidad de caída aumenta en promedio de ∼2.3 m/s a ∼4.0 m/s dentro de 300 m justo debajo de H0, revelando la fusión de los hidrometeoros. Por lo tanto, durante las tormentas, es posible determinar la altura de la capa de fusión (también conocida como banda brillante), lo que, a su vez, permite estimar H0. Estos eventos muestran una buena concordancia con H0 a partir de ERA5. Sobre todo en invierno, esta región está expuesta a fenómenos hidrometeorológicos provocados por la actividad sinóptica de latitudes medias. Los ríos atmosféricos son responsables de hasta ∼50 % de la precipitación total anual, y algunos casos pueden inducir precipitaciones extremas. Por lo tanto, desde una perspectiva sinóptica, se analizan tres eventos de precipitación, observando la evolución de H0 cuando registra valores altos, valores bajos y también, considerando la cantidad máxima de precipitación diaria.

Palabras claves – Isoterma 0°C, Biobio, MRR, AMDAR, ERA5, Banda brillante

Abstract

We analyze inter-annual, monthly, synoptic, and sub-daily variability aspects of the 0°C isotherm height (H0), using ERA5 reanalysis, observations and estimates, over the coast of the Biobío Region, Chile (36.8°S, 73°W). This region lacks radiosonde-based H0 measurements, but here we use hourly H0 observation onboard aircraft taking off and landing at the Carriel Sur International Airport (SCIE, 36.77°S, 73.06°W) for the period 2017-2019. We validate H0 from the reanalysis using observations, which reveals an excellent performance of ERA5 in resolving observations. H0 varies throughout the year with a maximum in January and a minimum in July. Then, we estimate H0 based on Micro Rain Radar data acquired at the Atmospheric River Observatory in Concepcion for 2022 and 2023 with high vertical and temporal resolution. In particular, we use vertical profiles of fall velocity and reflectivity of hydrometeors during precipitation events. Fall velocity increases on average from ∼2.3 m/s to ∼4.0 m/s within 300 m just below H0, revealing melting hydrometeors. Hence, in precipitation storms, it is possible to determine the height of the melting layer (also known as the bright band), which, in turn, enables the estimation of H0. These events show a fair agreement with H0 from ERA5. Particularly in winter, this region is exposed to hydrometeorological events caused by mid-latitude synoptic activity. Atmospheric rivers are responsible for up to ∼50 % of the total annual precipitation, and some cases might induce extreme precipitation. Therefore, from a synoptic perspective, three precipitation events are analyzed, observing the evolution of H0 when it registers high values, low values and also, considering the maximum amount of daily precipitation.

Keywords – isotherm 0°C, Biobio, MRR, AMDAR, ERA5, Bright band

Índice general

Índice de cuadros

Índice de figuras

Capítulo 1

Introducción

1.1. Antecedentes

El conocimiento de la variabilidad de la altitud de la isoterma 0°C (H0) contribuye a la comprensión de la dinámica de las precipitaciones. Representa el límite entre la capa atmosférica que comprende de nieve derretida por debajo y la que contiene nieve/hielo por encima (Benarroch et al., 2020). El nivel de congelación (que corresponde a H0) es definido por la American Meteorological Society (AMS, 2021) como “el nivel más bajo en la atmósfera libre donde la temperatura del aire es de 0°C” . Así, la identificación del nivel en el que se produce la fusión permite reconocer las precipitaciones iniciadas por el hielo. Si consideramos terrenos elevados, este nivel es importante porque la respuesta hidrológica difiere dependiendo de si la precipitación es líquida (impactando directamente en el flujo) o sólida, donde la nieve contribuye a la acumulación (Marks et al., 2013), marcando una línea de nieve que separa el área que genera escorrentía directa dentro de una cuenca de la porción que recibe nieve (Ibañez et al., 2021; Garreaud, 2013; Minder and Kingsmill, 2013), posteriormente dicha acumulación libera agua de deshielo durante la estación seca (Shulgina et al., 2023). El término H0 se confunde a menudo con el término "línea de nieve"(Schauwecker et al., 2017), que se define como "la extensión límite actual de la nieve que cubre el suelo"(AMS, 2021). Por ello, comprender la fase de precipitación y la zona en la que se produce la transición de precipitación sólida a líquida es esencial para una gestión eficaz de los recursos hídricos y crucial para desarrollar planes de prevención y mitigación de riesgos ante posibles impactos hidrometeorológicos asociados a eventos de alta

H0 (potencialmente causantes de deslizamientos de tierra; Garreaud, 2013). Del mismo modo, los eventos de baja H0 tienen consecuencias sobre la agricultura y la ganadería, ya que las precipitaciones sólidas (granizo o nieve) pueden dañar los cultivos (Pechan et al., 2023).

Se puede obtener la H0 de diferentes maneras, y cada una tiene sus limitaciones. La forma más directa es a partir de observaciones, mediciones rutinarias de radiosonda (Mardones and Garreaud, 2020), pero la realización es costosa, otra forma directa, pero no constante en el tiempo, es a partir de datos meteorológicos registrados en aeronaves (Smith and Blaes, 2015); extrapolando la temperatura del aire cercana a la superficie (Ibañez et al., 2021) pero dependen de las tasas de lapso utilizadas. Para evitar las limitaciones temporales, es posible obtener H0 utilizando datos de reanálisis (García-Lee et al., 2024; Schauwecker et al., 2022), y derivándolo de perfiles verticales obtenidos con radares (Endries et al., 2018; Perry et al., 2018; Schauwecker et al., 2017).

Considerando la última forma mencionada, los registros de los perfiladores verticales (como un Micro Rain Radar (MRR)) pueden monitorizar el estado de la atmósfera hasta ∼6 km cada 30 segundos (METEK, 2008), obteniendo medidas de los parámetros de precipitación. Dado que en la atmósfera la transformación de precipitación sólida a líquida no es instantánea (Austin and Bemis, 1950; Leary and Houze, 1979; Harris et al., 2000), sino que se trata de un cambio gradual, conduce a una zona de transición que comprende hielo/nieve por encima y agua por debajo (Hooper and Kippax, 1950). El MRR es crucial para obtener información sobre la zona de transición, conocida como capa de fusión (ML, por sus siglas en inglés), donde la precipitación sólida se derrite, provocando así un máximo en la reflectividad radar, conocida como la banda brillante (BB; Harris et al., 2000; Matrosov, 2008; Lundquist et al., 2008; Pfaff et al., 2014). Dicha intensificación se produce cuando las partículas de hielo atraviesan el nivel de congelación (Hooper and Kippax, 1950) e inician un proceso de fusión, que conduce a la formación de gotas de agua en el exterior de los copos de nieve, causado por las variaciones en el factor dieléctrico del hielo y el agua (Fabry and Zawadzki, 1995; White et al., 2002). Este proceso provoca un aumento de la reflectividad detectada por el radar. Una vez finalizado el proceso de fusión, la gota de lluvia más densa desciende más rápidamente que el copo de nieve precedente (Battan, 1973; Schauwecker et al., 2017). Muchos estudios consideran que la H0 puede estimarse como la parte

superior del ML (Glickman and Walter, 2000; Sánchez-Diezma et al., 2000; Perry et al., 2018; Endries et al., 2018; Mehta et al., 2020; Ramadhan et al., 2021 (véase su primera figura)). Se han encontrado buenas correlaciones entre los parámetros MRR y las mediciones convencionales de precipitación en Alemania (Peters et al., 2002). El estudio de Perry et al. (2018) ha utilizado el MRR mediante un algoritmo para detectar la altitud de la ML (MLH, por sus siglas en inglés) en América del Sur, encontrando un valor medio de 4810 m sobre Cusco, Perú, y 4786 m sobre La Paz, Bolivia. Massmann et al. (2017), utilizaron dos MRR en Chile, como parte de la instrumentación para observaciones de precipitación orográfica en la cordillera de Nahuelbuta.

La Región del Biobío en Chile es la segunda región más poblada del país y la zona costera se ve comúnmente afectada por la llegada a tierra de Ríos Atmosféricos (RAs; Garreaud et al., 2024; Viale et al., 2018) y tormentas severas. Esto provoca desbordamientos de ríos, deslizamientos de tierras e inundaciones, así como diversas consecuencias sociales y económicas. A pesar de estos antecedentes, no existen lanzamientos rutinarios de radiosondas en esta zona, que se encuentra entremedio de lances realizados en Santo Domingo a 33.65°S y Puerto Montt a 41.43°S (Figura 2.1.1a; es decir, separados por más de ∼1000 km), lo que resulta en un desconocimiento de la estructura vertical de la atmósfera en el paso de sistemas frontales. Por esta razón, las observaciones más directas de H0 disponibles para nuestro análisis son las derivadas de los perfiles verticales de temperatura recogidos a través del programa global Aircraft Meteorological Data Relay (AMDAR), una iniciativa de la Organización Meteorológica Mundial destinada a poner a disposición de los centros meteorológicos operativos los datos meteorológicos medidos por aviones comerciales. En particular, hacemos uso de los datos AMDAR asociados al Aeropuerto Internacional Carriel Sur, situado a unos 7 km del MRR (Figura 2.1.1b). Asimismo, en Concepción (36.8°S, 73°O, 25 m snm; Garreaud et al., 2024) se implementó el primer Observatorio de Ríos Atmosférico (ORA) de Chile.

1.2. Área de estudio y contexto climático

La zona de estudio presenta un clima templado con influencia mediterránea (Sarricolea-Espinoza et al., 2017). La Región del Biobío se ubica en la zona centro-

sur de Chile, aproximadamente entre las latitudes 36.3°S y 38.3°S. Limita al norte con la Región de Ñuble, al sur con la Región de la Araucanía, al oeste con el Océano Pacífico y al este con la Cordillera de los Andes y Argentina (Figura 2.1.1b). La altura promedio de la Cordillera de los Andes disminuye desde ∼4000 msnm a 30°S hasta ∼1500 msnm a 40°S, y este hecho configura una precipitación costera sobre el área de estudio (Barrett et al., 2009).

Aquí, la precipitación media anual es de 985.7 mm (1991-2020), y el 54,7 % se concentra durante el invierno austral (Aceituno et al., 2021; Viale and Garreaud, 2015); como muestra la Figura Suplementaria A0.1a, donde los valores de precipitación mensual muestran un claro patrón estacional con máximos (mínimos) en los meses de invierno (verano), este comportamiento es típico de regiones con influencias mediterráneas, donde las lluvias están asociadas y causadas principalmente por frentes fríos y RAs (Garreaud, 2013). Durante eventos que exhiben principalmente flujo del noroeste se observan cantidades significativas de precipitación cerca de la costa, con impactos hidrometeorológicos (Valenzuela and Garreaud, 2019), como inundaciones y desbordes de ríos (Garreaud, 2013).

En esta zona, las alturas de los Andes alcanzan ∼3000 msnm, y la región entre 35°S y 38°S exhibe un gradiente de precipitación zonal desde la costa hacia los Andes debido a efectos orográficos, lo que conduce a la acumulación de nieve sobre los Andes (Barrett et al., 2009; Garreaud, 2009; Viale and Garreaud, 2015; Valenzuela and Garreaud, 2019). En la región del Biobío, la principal cuenca hidrográfica corresponde a la del río Biobío (Yevenes et al., 2018); durante su curso desde los Andes hacia el océano Pacífico, el agua es extraída para usos humanos, como actividades relacionadas con la silvicultura y la agricultura (Grantham et al., 2013).

1.3. Objetivos e hipótesis

Dentro del contexto que engloba esta investigación, se llevaron a cabo dos preguntas científicas:

P1: ¿Cuál es el error asociado al estimar la altitud de la isoterma 0°C que entrega el análisis de datos adquiridos desde el Micro Rain Radar en relación a las observaciones directas de AMDAR y otras fuentes de datos de los cuales se obtienen dicha variable?

P2: ¿La caracterización de la variabilidad de la altitud de la isoterma 0°C nos permite una mejor comprensión sinóptica de eventos extremos?

Por lo tanto, las preguntas científicas llevan a la siguiente hipótesis: "Los registros de Banda Brillante obtenidos del MRR permiten cuantificar la altitud y variabilidad sub-diaria, inter-diaria y estacional de la isoterma 0^{o}C, y éstas son comparables con la información derivada de observaciones AMDAR, y datos de reanálisis".

De esta forma, el objetivo general este trabajo es analizar la variabilidad de la Banda Brillante y la altitud de la isoterma 0°C durante eventos de precipitación a escala inter-diaria, sub-diaria y estacional sobre la zona costera del Biobío a través de un análisis comparativo de distintas fuentes. Para cumplir con el objetivo general, se deben seguir lo siguiente:
1. Obtener la Banda Brillante (BB) observada por el Micro Rain Radar (MRR) y estimar la altitud de isoterma 0°C (H0) desde diferentes fuentes (AMDAR, reanálisis ERA5 y MRR).
2. Realizar un análisis comparativo entre las estimaciones de la H0 (AMDAR, reanálisis ERA5 y MRR), con la intención de validar la estimación de la H0 a partir del MRR.
3. Describir la variabilidad a escala inter-diaria, sub-diaria y estacional de BB y H0 obtenidas de las diferentes fuentes, para eventos con y sin precipitación sobre la zona de estudio.
4. Identificar y caracterizar las configuraciones sinópticas que se relacionan con eventos específicos de H0 en la zona de estudio.

El capítulo siguiente es un manuscrito enviado a la revista International Journal of Climatology, titulada: *Temporal variability of the 0°C isotherm height over the coast of the Biobío Region (36.8^{o}S), Chile: characterization and case studie*, el cual cuenta con una primera sección de introducción, seguida de una presentación de información acerca del contexto climático y el área de estudio, luego se presentan los datos y métodos en la sección 2.3, se describen los resultados en la sección 2.4. La sección 2.5 aborda casos de estudios junto con sus principales patrones sinópticos. Se presenta en la sección 2.6 la conclusión.

Capítulo 2

Temporal variability of the 0°C isotherm height over the coast of the Biobío Region (36.8ºS), Chile: characterization and case studies

2.1. Introduction

Knowledge on the 0°C isotherm height (H0) variability contributes to the understanding of precipitation dynamics. It represents the boundary between the atmospheric layer comprising melted snow below and that containing snow and ice above (Benarroch et al., 2020). The freezing level (which corresponds to H0) is defined by the American Meteorological Society (AMS, 2021) as "the lowest level in the free atmosphere where the air temperature is 0°C". Thus, identifying the level at which melting occurs, makes it possible to recognize ice-initiated precipitation. If we consider elevated terrains, this level is important because the hydrological response differs depending on whether the precipitation is liquid (directly impacting the flow) or solid, where snow contributes to accumulation (Marks et al., 2013), marking a snowline that separates the area that generates direct runoff within a watershed from the portion that receives snow (Ibañez et al., 2021; Garreaud, 2013; Minder and Kingsmill, 2013), subsequently such accumulation releases meltwater during the dry season (Shulgina et al., 2023).

The term H0 is often confused with the term "snowline" (Schauwecker et al., 2017), which is defined as "the current boundary extent of snow covering the ground" (AMS, 2021). That is why understanding the precipitation phase and the zone where the precipitation transition from snow-rain occurs, is essential for effective water resource management and crucial for developing prevention and risk mitigation plans for potential hydrometeorological impacts associated with high H0 events (potentially causing mudslides; Garreaud, 2013). Similarly, low H0 events have consequences on agriculture and livestock, since solid precipitation (hail or snow) can damage crops (Pechan et al., 2023).

H0 can be obtained in different ways, and each has its limitations. The most direct way is from radiosonde observations (Mardones and Garreaud, 2020), keeps regulated measurements but is expensive, another directly way, but not constant in time, is from meteorological data recorded in aircraft (Smith and Blaes, 2015); by extrapolating near-surface air temperature (Ibañez et al., 2021) but they depend on the lapse rates used. To avoid temporal limitations, it is possible to obtain H0 by using reanalysis data (García-Lee et al., 2024; Schauwecker et al., 2022), and by deriving it from vertical profiles obtained with radars (Endries et al., 2018; Perry et al., 2018; Schauwecker et al., 2017).

Considering the last way, the vertical profilers (as a Micro Rain Radar (MRR)) records can monitor the state of the atmosphere up to ∼6 km every 30 seconds (METEK, 2008), obtaining measurements of rainfall parameters (see section 2.4). Since in the atmosphere the transformation from solid to liquid precipitation is not instantaneous (Austin and Bemis, 1950; Leary and Houze, 1979; Harris et al., 2000); instead, it is a gradual change, leading to a transition zone comprising ice/snow above and water below (Hooper and Kippax, 1950). MRR is crucial to obtain information about the transition zone, known as the melt layer (ML), where precipitation in the form of ice melts, hence causing a maximum in the vertical profile radar reflectivity known as the bright band (BB; Harris et al., 2000; Matrosov, 2008; Lundquist et al., 2008; Pfaff et al., 2014). The intensification of the corresponding echo occurs when ice particles cross the freezing level (Hooper and Kippax, 1950) and initiate a melting process, leading to the formation of water droplets on the exterior of snowflakes, caused by variations in the dielectric factor of ice and water (Fabry and Zawadzki, 1995; White et al., 2002). This process causes an increase in reflectivity detected by the radar. After the melting

process finishes, the denser raindrop descends faster than the preceding snowflake (Battan, 1973; Schauwecker et al., 2017). Many studies consider that the H0 can be estimated as the top of the ML (Glickman and Walter, 2000; Sánchez-Diezma et al., 2000; Perry et al., 2018; Endries et al., 2018; Mehta et al., 2020; Ramadhan et al., 2021 (see their first figure)). Good correlations have been found between MRR parameters and conventional precipitation measurements in Germany (Peters et al., 2002). It has also been used to detect the ML height (MLH) using an algorithm in South America, finding a mean value of 4810 m over Cusco, Peru, and 4786 m over La Paz, Bolivia Perry et al. (2018). Massmann et al. (2017), used two MRRs in Chile, as part of the instrumentation for observations of orographic precipitation in the Nahuelbuta mountain range.

The Biobío Region in Chile is the second most populated region in the country and the coastal zone is commonly affected by landfalling Atmospheric Rivers (ARs; Garreaud et al., 2024; Viale et al., 2018) and severe storms (see section 2.2). This causes river overflows, landslides and flooding, as well as several social and economic consequences. Despite this background, there are no routine radiosonde launches in this area, which is midway between routine launches twice a day in stations separated by ∼1000 km (Santo Domingo at 33.65°S and Puerto Montt at 41.43°S; Figure 2.1.1a), which results in a lack of knowledge about the vertical structure of the atmosphere in the passage of frontal systems. For this reason, the most direct observations of H0 available for our analysis are those derived from temperature vertical profiles gathered through the global Aircraft Meteorological Data Relay (AMDAR) program, a World Meteorological Organization initiative aimed at making meteorological data measured by commercial aircraft available to operational weather centers. In particular, we make use of AMDAR data associated to the Carriel Sur International Airport, located approximately 7 km away from the MRR (Figure 2.1.1b). Also, the first Atmospheric River Observatory (ORA) in Chile was implemented in Concepción (36.8°S, 73°W, 25 m asl; Garreaud et al., 2024).

This study aims: 1) To describe the H0 in the study area using AMDAR data, 2) To obtain the climatology of H0 once the validation of the ERA5 reanalysis data has been done, and 3) Study whether MRR data allows to characterize temporal variability of H0 during winter storms reaching the Biobio region. The latter has important practical applications since data from the MRR at Concepcion provides

the only estimate of H0 available in real-time.

Section 2.2 provides information about the study area and the climate context during the study period. Data and methods are presented in section 2.3; results are described in section 2.4. Section 2.5 addresses case studies, with a focus on their corresponding synoptic patterns. Conclusions remarks are presented in section 2.6.

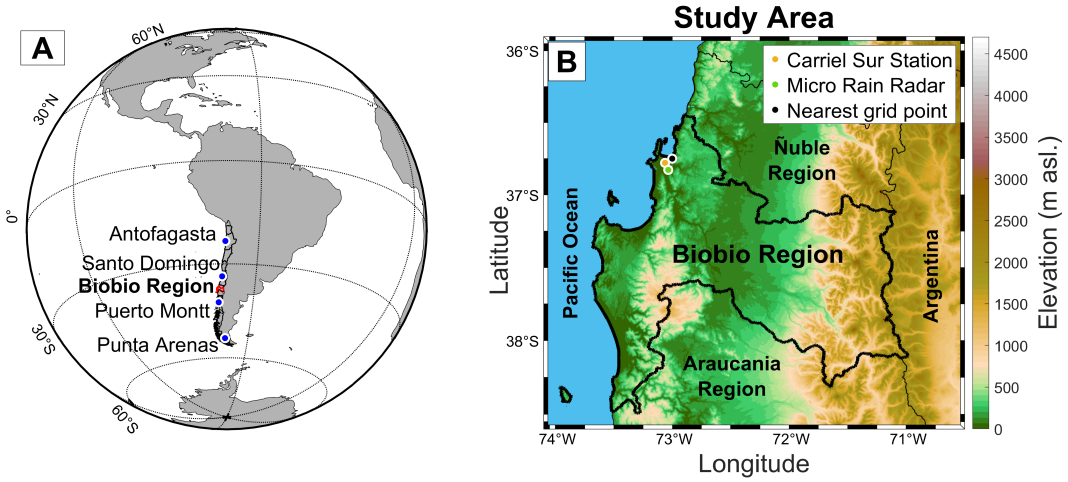

Figura 2.1.1: A) Geographical location of the Biobío Region (red boundary) along with the locations of the routine radiosonde launches in Antofagasta, Santo Domingo, Puerto Montt and Punta Arenas (blue dots). B) Study area, Biobío Region, the dark yellow dot corresponds to the location of the Carriel Sur station in Talcahuano, the dark green dot corresponds to the location of the Micro Rain Radar in Concepción and the black dot corresponds to the closest grid point of ERA5.

2.2. Study area and climate context

The study area exhibits a temperate climate with a Mediterranean influence (Sarricolea-Espinoza et al., 2017). The Biobío Region is located in central-south Chile, roughly between 36.3°S and 38.3°S. Its boundaries are the Ñuble Region to the north, the Araucanía Region to the south, the Pacific Ocean to the west, and the Andes mountains and Argentina to the east (Figure 2.1.1b). The mean height of the Andes decreases from ∼4000 m asl at 30ºS to ∼1500 m asl at 40°S, and this fact shapes a coastal precipitation on the area study (Barrett et al., 2009).

Here, the mean annual precipitation is 985.7 mm (1991-2020), and 54.7 % is concentrated during the austral winter (Aceituno et al., 2021; Viale and Garreaud, 2015); as shown by Supplementary Figure A0.1a, monthly precipitation value exhibits a clear seasonal pattern, with a maxima (minima) concentrated during the winter (summer) months, this behavior is typical of regions with mediterranean influence, where the precipitation is associated and mainly caused by cold fronts and ARs (Garreaud, 2013). During events exhibiting primarily northwesterly (NW) flow significant amounts of precipitation near the coastline are observed, with hydro-meteorological impacts (Valenzuela and Garreaud, 2019), such as floods and river overflows (Garreaud, 2013).

In this zone, the Andes heights reach ∼3000 m asl, and the region between 35°S and 38°S exhibits a zonal precipitation gradient from the coast toward the Andes due to orographic effects, leading to snow accumulation over the Andes (Barrett et al., 2009; Garreaud, 2009; Viale and Garreaud, 2015; Valenzuela and Garreaud, 2019). In the Biobío region, the main watershed corresponds to the Biobío River basin (Yevenes et al., 2018); during its course from the Andes into the Pacific Ocean, water is extracted for human uses, such as activities related to forestry and agriculture (Grantham et al., 2013).

2.3. Data and methods

2.3.1. Precipitation

The Dirección Meteorológica de Chile (DMC, for its acronym in Spanish) maintains a long-term weather station at the Carriel Sur International Airport (36.77°S, 73.06°W, 17m; dark yellow point on Figure 2.1.1b). Hourly values correspond to the accumulated sum for 1-hour periods ending at the reported hour. The periods 2017-2019 and 2022-2023 are considered. We defined “wet hours” as those recording over or equal to 0.5 mm, otherwise, we use the term “dry hours”. The 0.5 mm threshold was chosen taking into account that a wet day is considered as those days with rainfall mm (Valenzuela and Garreaud (2019)), therefore, in terms of hourly scale we chose that at least in the recorded hour, the rain gauge shows a value equal or higher than 0.5 mm. For 2017-2019 we identified 450 wet hours, and for 2022-2023 there are 722 wet hours. Supplementary Figure A0.1b show the accumulated precipitation curves, the year analyzed in this study show a

lower accumulation compared to the climatology. Among these, 2017 is the closest to the climatology, whereas 2019 exhibits the largest deficit, with approximately 300 mm less.

2.3.2. H0 derived from ERA5 Reanalysis data ($H0_{ERA5}$)

Hourly H0 values were retrieved from ERA5 (zero-degree level), the fifth-generation atmospheric reanalysis from the European Center for Medium-Range Weather Forecasts (ECMWF). Its horizontal resolution is 0.25° x 0.25° (roughly 31 km) and covers the period from 1950 to the present (Hersbach et al., 2020). $H0_{ERA5}$ represents the height above the ground level where the temperature changes from positive to negative values (C3S, 2017), and thus it is necessary to add the topographic elevation to obtain $H0_{ERA5}$ in meters above sea level (m asl; Schauwecker et al., 2017). The topographic elevation is 118.9 m in the study area, considering the nearest grid point (36.75°S, 73°W; black point on Figure 2.1.1b).

2.3.2.1. Other variables from ERA5

Additionally, we used the values of total precipitation on the study area (same nearest grid point) for the period 1991-2020 to obtain the climatology of H0 in dry and wet hours. For synoptic conditions, we used hourly values of total column precipitable water (PW; kg/m^2) and integrated water vapor transport (IVT vector; kg/ms), as well as geopotential height at 300 hPa (GH; dm) and mean sea level pressure (SLP; hPa). All variables were retrieved for the 10°S - 60°S and 120°W - 50°W domains and at 12 UTC (Table 2.3.1).

2.3.3. H0 derived from AMDAR data ($H0_{AMDAR}$)

The AMDAR program is crucial as a provider of aerological information beyond the sparse operational global radiosonde network (Stickland and Grooters, 2005), especially near busy airports. AMDAR temperature profiles retrieved for airplanes landing and taking off at Carriel Sur airport were processed with the same methodology described by Muñoz et al. (2022), which included the computation of heights using the hypsometric equation based on pressures and temperatures of each profile and the use of the surface meteorological station data to extend the profiles down to the surface. A total of 6497 hourly vertical profiles of temperature were available for the 2017-2019 period, averaging over 1-hour periods, from which

H0 was estimated with a simple linear interpolation. While a large fraction of the days in the period has data (89 %), the diurnal availability is concentrated in the daytime hours from 10 to 03 UTC (See Supplementary Figure A0.2) when most of the commercial domestic airplanes operate. Due to the weak diurnal cycle at the typical H0 altitudes in the region, this lack of nocturnal observations is not expected to be a major limitation of our analysis. AMDAR data for the Carriel Sur airport after 2019 is due to the COVID-19 pandemic and eventually becomes non-existent after 2020 when the national airline providing the data terminated its participation in the program.

2.3.4. H0 derived from MRR data ($H0_{MRR}$)

The Micro Rain Radar MRR-2, built by METEK (Germany), was installed in April 2016 at the facilities of the University of Concepcion. It uses electromagnetic radiation with a frequency of 24 GHz to retrieve vertical profiles of precipitation parameters: path integrated attenuation (dBz), attenuated radar reflectivity (hereafter just reflectivity Z; dBz), radar reflectivity (dBz), rain rate (mm/h), liquid water content (g/m^3) and fall velocity (W; m/s) (METEK, 2008). The data is collected every 2 minutes and saved in separate files every 24 hours. The radar has been measuring since April 2022 with two resolutions: every 100 meters between 100 and 3100 meters, and every 250 meters between 250 and 7750 meters. Between 2016 and 2019, measurements for the first height span were taken every 50 m between 50 m and 1500 m, keeping the resolution for the second height span. In this study, only the resolution from April 2022 onwards is considered because the measurement every 50 m did not capture the level where melting occurs. Both resolutions are combined to achieve a single resolution of 100 m between 100 and 2500 m, and 250 meters from 2500 to 6000 m. We decided to limit the vertical extent to 6000 m because the MRR data showed noise between 6000 m and 7750 m, which could affect the derivation of H0. The noise was detected by examining the radar variable images, which was initially used as a visual filter to determine the ML (Brast and Markmann, 2020), identified by its continuity in time and later contrasted with the derived $H0_{MRR}$. Then, consider the top of the ML as the H0.

In this study, we applied the algorithm based on the methodology described by Schauwecker et al. (2017) originally applied in the Peruvian Andes. This algorithm involves a series of steps to derive the melting layer height (MLH). First, positive

gradients of Z and W (i.e., increasing with height) are discarded. The hydrometeors must reach the surface to estimate H0. Therefore, the second step is to remove periods of virga (continuous data between 300 and 1500 m in the vertical) which are hydrometeors that fall but evaporate in the lower troposphere. Third, the most negative gradients of Z (NGZ) and W (NGW) are identified. Additionally, periods where the NGZ is not found within 3 levels above the NGW are discarded. The fifth and sixth steps involve identifying the bottom of this layer as the NGW and the top as the NGZ (Perry et al., 2017; Endries et al., 2018). Then, the average melting layer thickness (MLT) is calculated as the difference between the NGZ and NGW. Finally, the MLH is calculated as the sum of the height of the NGW and the average MLT. In the last two steps, it is ensured that the MLH is calculated below 6000 meters and heights outside one standard deviation from the mean of each hour are discarded (See Supplementary Figure A0.3). After that, $H0_{MRR}$ is available at 2-minutes resolution. To compute hourly means, we considered a data completeness criteria of at least 7 data points (∼25 %) in an hour. By definition, data is only available for wet conditions.

For the period 2022-2023, ∼79.7 % of the days are available from MRR data. Considering observations every 2 minutes and after applying the algorithm, 8241 precipitation signals were identified by the radar and met the necessary conditions to calculate H0. These values correspond to 109 days where the ML is visually identified. After considering the criteria applied for data completeness, we identified 363 wet hours (corresponding to 97 days).

The use of radars in meteorological studies has been an important tool worldwide (Ghada et al., 2022; Garcia-Benadi et al., 2022; Ramadhan et al., 2021; Brast and Markmann, 2020; Mehta et al., 2020; Seidel et al., 2019; Boodoo et al., 2010). Specifically, MRR and AMDAR are non-traditional observation platforms that provide valuable information for the description of atmospheric processes (Smith and Blaes, 2015). Obtaining aerological data in specific regions is challenging and costly but also necessary to understand precipitation processes.

2.3.5. H0 derived from radiosonde ($H0_{RSONDE}$)

In July 2022, a radiosonde campaign (RC) was conducted at the location of the MRR to complement surface measurements (Garreaud et al., 2024). We will use these observations as an additional direct measurement of $H0_{RSONDE}$ to contrast

$H0_{MRR}$. There are 18 hours of data available from July 8 to July 24, 2022 (see Table 2.3.1).

<table>
<tr><th>Source</th><th colspan="2">Variable; name</th><th>Spatial resolution/ level</th><th colspan="2">Temporal resolution; available data (date)</th></tr>
<tr><td>DMC</td><td colspan="2">Precipitation; pp (mm)</td><td>Superficial point; (73.06°W; 36.77°S)</td><td colspan="2">Hourly; 01/08/2018 - 31/12/2023</td></tr>
<tr><td>AMDAR</td><td colspan="2">Altitude of the isotherm 0°C; $H0_{AMDAR}$ (m. asl.)</td><td>Vertical point; (73.06°W; 36.77°S)</td><td colspan="2" rowspan="5">Hourly; 01/01/2017 - 31/12/2019

Hourly; 01/01/2022 - 31/12/2023</td></tr>
<tr><td rowspan="4">ERA5</td><td colspan="2">Zero degrees level; $H0_{ERA5}$ (m agl.)</td><td>Vertical point; (73°W; 36.75°S)</td></tr>
<tr><td colspan="2">Precipitable water; PW* (mm)</td><td rowspan="3">0.25° x 0.25° / superficial</td></tr>
<tr><td colspan="2">Integrated water Vapor Transport; IVT vectorial* (kg/m/s)</td></tr>
<tr><td colspan="2">Sea level pressure; SLP* (hPa)</td></tr>
<tr><td colspan="2">Geopotencial; GH* (dm)</td><td>0.25° x 0.25° / 300 hPa</td></tr>
<tr><td rowspan="2">MRR</td><td>Reflectivity; Z (dBZ)</td><td rowspan="2">$H0_{MRR}$ (m asl.)</td><td rowspan="8">Vertical point; (73.03°W; 36.8°S)</td><td colspan="2" rowspan="2">Per minute and hourly; 19/04/2022 - 31/12/2023</td></tr>
<tr><td>Fall velocity; W (m/s)</td></tr>
<tr><td rowspan="7">Radio-sonde</td><td colspan="2" rowspan="7">Altitude of the isotherm 0°C; $H0_{RSONDE}$ (m. asl.)</td><td>Day</td><td>Hour (UTC)</td></tr>
<tr><td>08</td><td>20</td></tr>
<tr><td>09</td><td>04-12-20</td></tr>
<tr><td>10</td><td>04-12</td></tr>
<tr><td>16</td><td>18</td></tr>
<tr><td>17**</td><td>00-06-12-18**</td></tr>
<tr><td>23</td><td>12-18</td></tr>
<tr><td>24</td><td>00-06-12-18</td></tr>
</table>

Cuadro 2.3.1: Description of data sources. *Obtained through R-Explorer. **Hours used in Figure 2.4.3.

2.3.6. Validation of $H0_{ERA5}$ using $H0_{AMDAR}$ and comparison with $H0_{MRR}$

To compare the $H0_{ERA5}$ data with the $H0_{AMDAR}$ dataset for the period 2017-2019, and subsequently with the $H0_{MRR}$ dataset, we used statistical metrics, such as correlation (r), determination coefficient (R^2), root mean square error (RMSE),

and mean absolute error (MAE), following Wilks (2011) and Monte Carlo method is used for statistical significance. Also, the values of total precipitation from ERA5 is validated with hourly precipitation data from Carriel Sur station for the year 2017 to 2023, resulting in values of 0.6, 0.35 and 0.06 in correlation, RMSE and MAE, respectively (all statistically significant).

The $H0_{AMDAR}$ has hourly temporal resolution, and comparisons with $H0_{MRR}$ are initially conducted at this resolution. For a comprehensive variability description, we also analyze monthly means, considering dry and wet hours separately each month. Seasonal means are constructed for austral summer (December - January - February, DJF), autumn (March - April - May, MAM), winter (June - July - August, JJA), and spring (September - October - November, SON).

2.4. Results

2.4.1. Observations from AMDAR

First, we describe the $H0_{AMDAR}$ observations, Figure 2.4.1a (dark yellow dots) shows a seasonal pattern in the period 2017-2019, with maximum (minimum) values in summer (winter), averaging ∼4100 m (∼2500 m). Due to the short period, there is no trend in the data, however, the variability between years it is observed that during the first months of the period corresponding to summer, it is warmer on average than subsequent summers, while winters the differences are minimal, remaining constant year after year at the same altitude of ∼2500 m.

We identified 4921 dry hours with a mean of ∼3400 m asl with a range between ∼1100 m and ∼5700 m asl (Figure 2.4.1c). Also, we identified 88 wet hours (blue points on Figure 2.4.1b) and its majority (52 %) occurred during winter (JJA). $H0_{AMDAR}$ during wet hours shows an average of ∼2200 m asl with values ranging between ∼880 m and ∼3800 m asl (Figure 2.4.1c). The typical value of $H0_{AMDAR}$ in the study area on dry hours is 3500 m asl, while on wet hours is 2200 m asl (See Supplementary Figure A0.4a and A0.4c).

2.4.2. Validation of reanalysis data

Here we compare $H0_{AMDAR}$ and $H0_{ERA5}$ for the period 2017-2019. Their correlation coefficient reaches 0.98 using all hours available. As shown in Figure 2.4.1b,

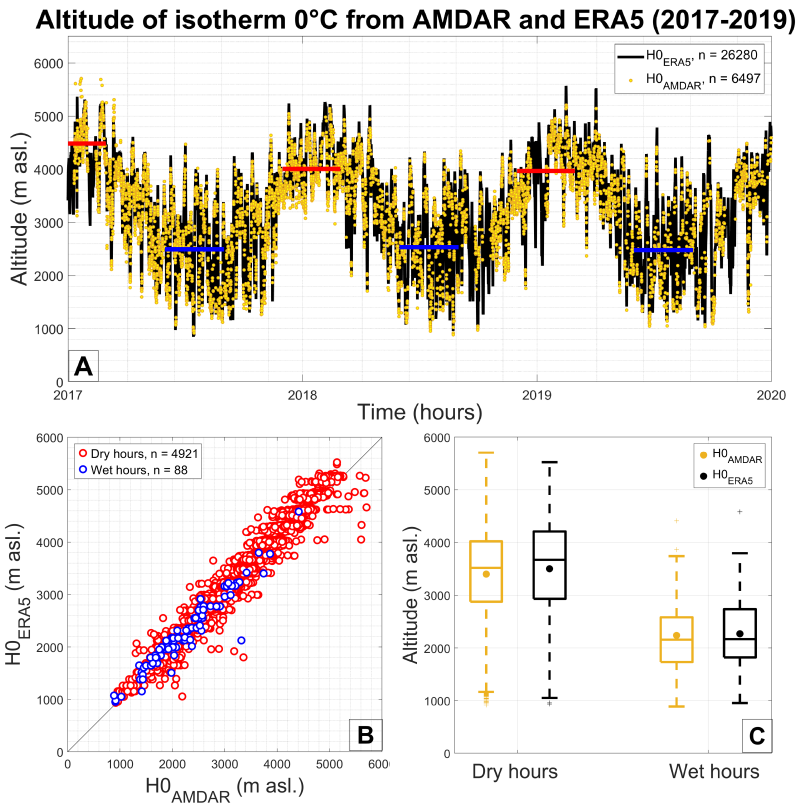

Figura 2.4.1: A) Time series of $H0_{ERA5}$ (in black) and $H0_{AMDAR}$ (in dark yellow); the red (blue) horizontal lines correspond to the $H0_{AMDAR}$ averages of the summer (winter) season corresponding to each year. B) Scatter plot between $H0_{AMDAR}$ and $H0_{ERA5}$ for dry hours (red dots) and wet hours (blue dots) recorded at Carriel Sur station. C) Same as B but in box plot.

considering dry hours (red circles), both datasets show a strong positive linear correlation ($R^2 = 0.97$) with little dispersion, although in some instances $H0_{ERA5}$ underestimates the observations. Additionally, the RMSE and MAE values obtained for $H0_{ERA5}$ with respect to $H0_{AMDAR}$ are 194 and 148 m, respectively. Compared wet hours from $H0_{AMDAR}$ with $H0_{ERA5}$, values below 4000 m exhibit a positive linear correlation ($R^2 = 0.88$). See more information for statistical metrics in Table 2.4.1. As anticipated in comparison to dry hours, during wet hours the mean decreases slightly for both estimates. Additionally, $H0_{ERA5}$ monthly means remain higher than $H0_{AMDAR}$ (See Supplementary Figure A0.4b and A0.4d). Therefore, we conclude that ERA5 accurately described the H0 variability on the coastal area of the Biobío Region.

Period	Statistics		Dry hours	Wet hours
2017 - 2019	r		0.98*	0.96*
	R^2		0.97*	0.88*
	RMSE (m asl.)		194*	197*
	MAE (m asl.)		148*	133*
	Mean	$H0_{AMDAR}$	3400	2200
		$H0_{ERA5}$	3500	2200
2022 - 2023	r		-	0.77*
	R^2		-	0.59*
	RMSE (m asl.)		-	450*
	MAE (m asl.)		-	245*
	Mean	$H0_{MRR}$	-	2000
		$H0_{ERA5}$	-	2200

Cuadro 2.4.1: Statistics. For both periods and conditions (dry and wet hours). Between $H0_{AMDAR}$ and $H0_{ERA5}$ for 2017-2019 and between $H0_{MRR}$ and $H0_{ERA5}$ for 2022 and 2023. *Statistically significant.

2.4.3. Climatology of $H0_{ERA5}$

As $H0_{ERA5}$ was validated with AMDAR data, we now describe the climatology of $H0_{ERA5}$ from 1991 to 2020. The 30-year time series (Figure 2.4.2a) shows a marked seasonal variability; during the winter months a decrease in H0 (blue dots) is observed, reaching averages close to 2500 m asl. In contrast with the summer months (red points), H0 rises on average to 4000 m asl, revealing warm conditions typical of the season. As for the trend (Figure 2.4.2b), there is an increase of 95 m/year in the annual trend during the 30 years, with a positive (negative) trend observed during the DFJ, MAM and SON months (JJA).

As noted in section 4.2, wet hours tend to have lower H0 values than dry hours and in the climatology of $H0_{ERA5}$ this difference is clearly observed (Figure 2.4.2c). In the month of January this difference is greater with respect to the winter months, where they remain at a similar average value. The number of wet hours increases towards the winter months and shows less dispersion in the warm months and greater variability is observed in the cold months.

2.4.4. Detecting falling hydrometeors

Before analyzing the $H0_{MRR}$ variability, we tested the results of the corresponding estimation algorithm on the specific day: July 17, 2022, with known synoptic

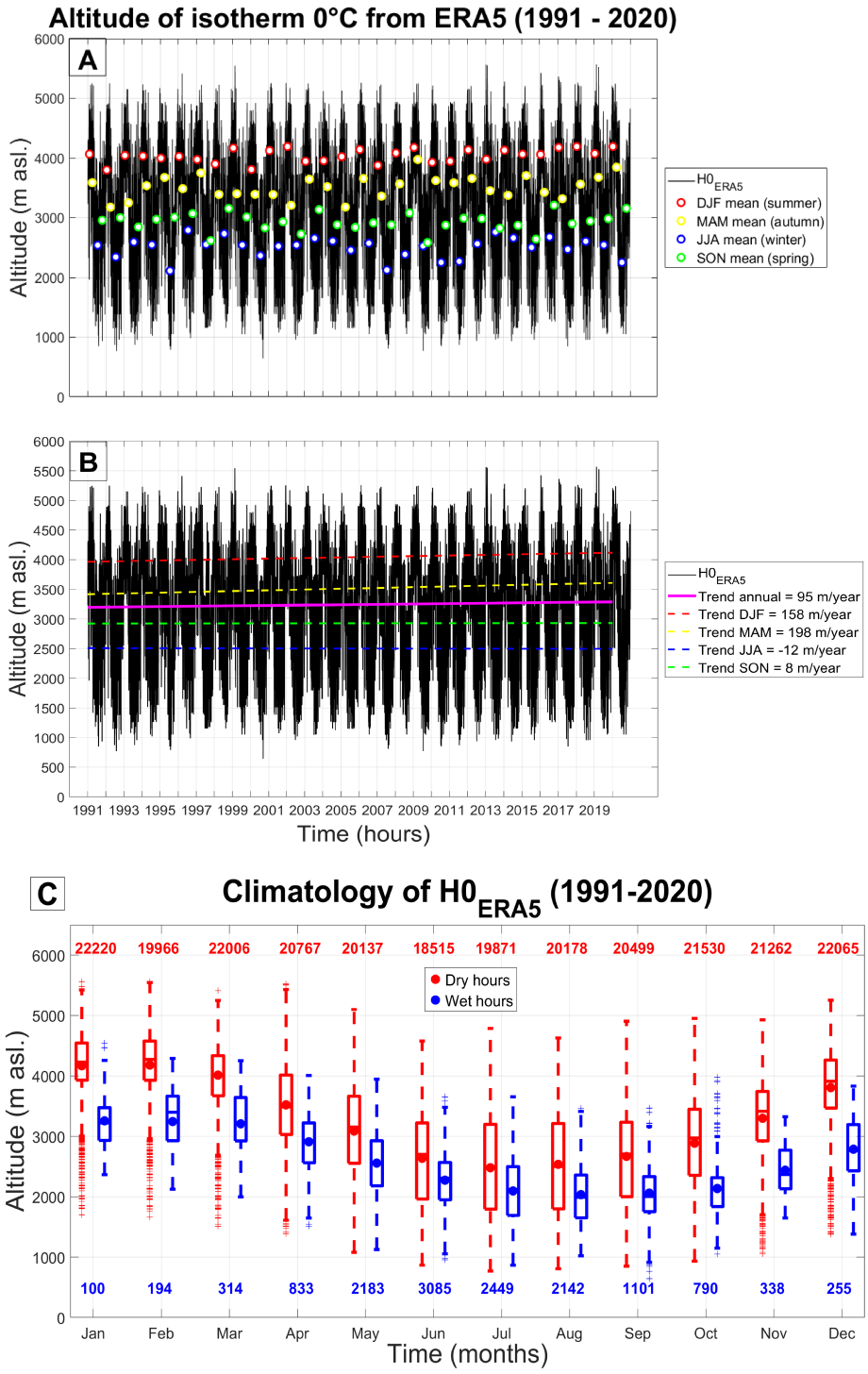

Figura 2.4.2: A) Time 30-year serie of H0 from ERA5 data (1991 - 2020) for season. B) Tendency of H0 from ERA5 annual (magenta), DJF (red), MAM (yellow), JJA (blue) and SON (green). C) Climatology of H0 from ERA5 data (1991 - 2020) for dry (red) and wet (blue) hours. Dots correspond to monthly averages.

conditions: a long and narrow atmospheric river with accumulated rainfall over 30 mm and IVT over 400 kg/ms in zonal direction described in Garreaud et al. (2024). Figure 2.4.3 shows that day, when radiosonde launches were conducted at 00, 06, 12 and 18 UTC, recording $H0_{RSONDE}$ of 1252, 1208, 2175 y 1846 m asl, respectively. The total daily precipitation accumulation reached 42 mm. $H0_{MRR}$ accurately estimates the reflectivity curve recorded by the MRR, indicating solid precipitation values below 20 dBZ and liquid precipitation above 30 dBZ. There is an observed increase in H0 from ∼1000 m asl (between 04 and 07 UTC) to ∼2000 m asl (between 10 and 17 UTC) as precipitation accumulates (peaking at 13 UTC with 6.8 mm accumulated in 1 hour). The daily mean $H0_{MRR}$ corresponds to ∼1700 m asl, while for $H0_{ERA5}$ indicates ∼1650 m asl. Regarding the BB, Figure 2.4.3b exhibits an average velocity at its top (bottom) of 2.3 m/s (4 m/s). Additionally, the thickness of the layer is ∼230 m. $H0_{MRR}$ and $H0_{ERA5}$ showed a strong positive correlation during this day, with $R^2 = 0.96$ (15 data points). Also, the statistical metrics between $H0_{MRR}$ and $H0_{ERA5}$ are described on Table 2.4.1.

Given these results, we now use the algorithm for the whole of 2022 and 2023. As shown in Figure 2.4.4a, $H0_{MRR}$ has an average of ∼2000 m asl, also we note that the winter mean is ∼1700 m for 2022 and for 2023 is ∼2300 m asl. Figure 2.4.4b shows H0 estimated from MRR and ERA5, showing a good overall agreement for wet hours: $R^2 = 0.59$. Figure 2.4.4b shows $H0_{ERA5}$ values above 1000 m with respect to $H0_{MRR}$, showing that the reanalysis overestimates the H0 estimates from radar. Similar results of the ERA5 reanalysis were obtained in García-Lee et al. (2024) and Schauwecker et al. (2022).

In addition, we note that the year 2023 (Figure 2.4.4a) has higher H0 values, which will affect the results with respect to the climatology obtained from $H0_{ERA5}$. However, since we have the most data during the winter months (JJA), the mean of ∼2000 m asl is representative. Additionally, by exploring wet hours in MRR data, the monthly average of the BB is derived for 2022 and 2023 (See Supplementary Figure A0.5). The BB has a mean thickness of ∼170 m between its top (H0) and its bottom. We see that, on average, a hydrometeor must fall about 170 m asl to melt and gradually increase its fall velocity from ∼2.3 m/s to ∼4 m/s (Figure 2.4.5).

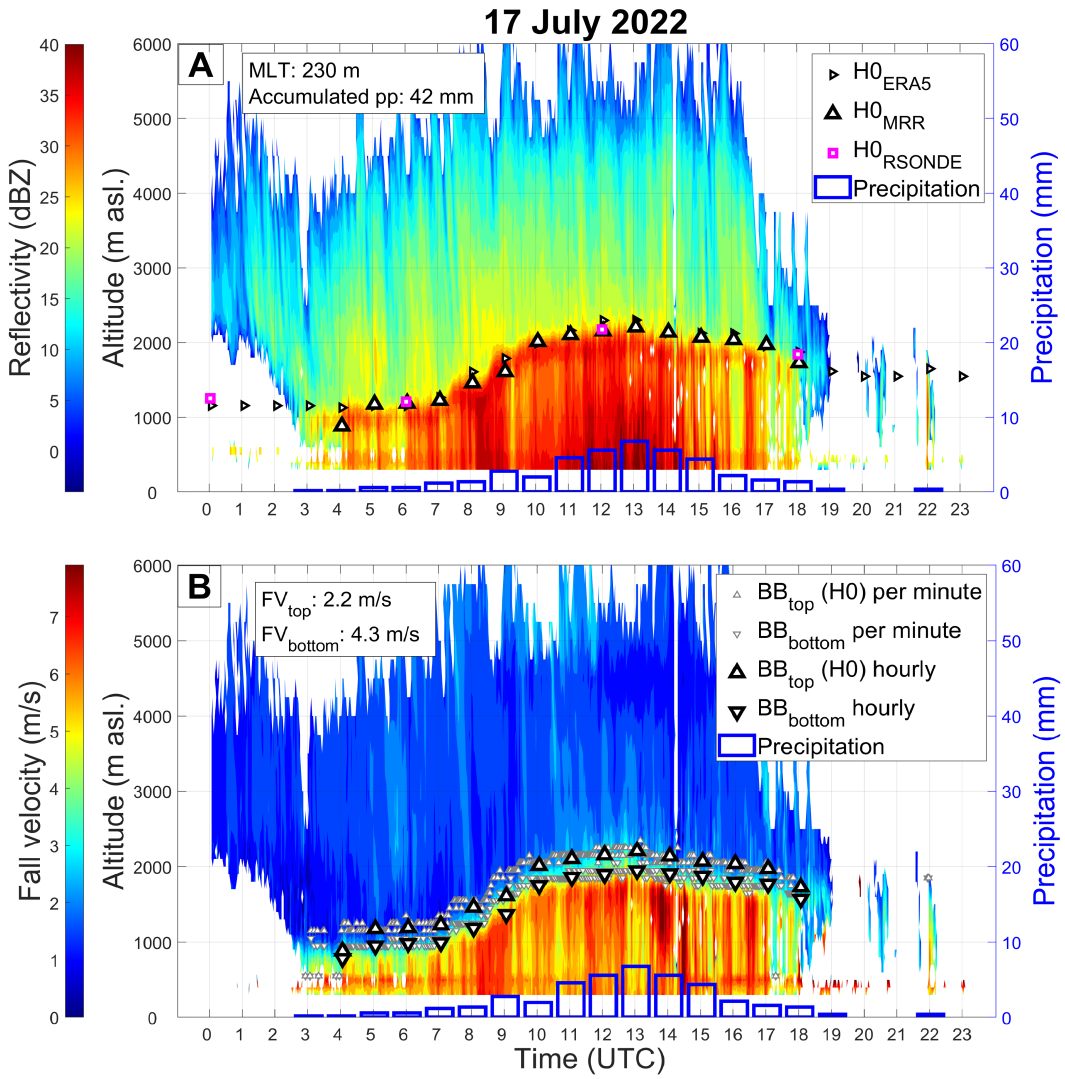

Figura 2.4.3: July 17, 2022. A) Reflectivity (measured in dBZ) recorded by the MRR, the triangles is for hourly scale, the rotated triangles corresponds to the $\mathbf{H0_{ERA5}}$, the magenta squares are the $\mathbf{H0_{RSONDE}}$ and the blue bars correspond to precipitation. B) Fall Velocity (FV; measured in m/s) recorded by the MRR, top and bottom of BB.

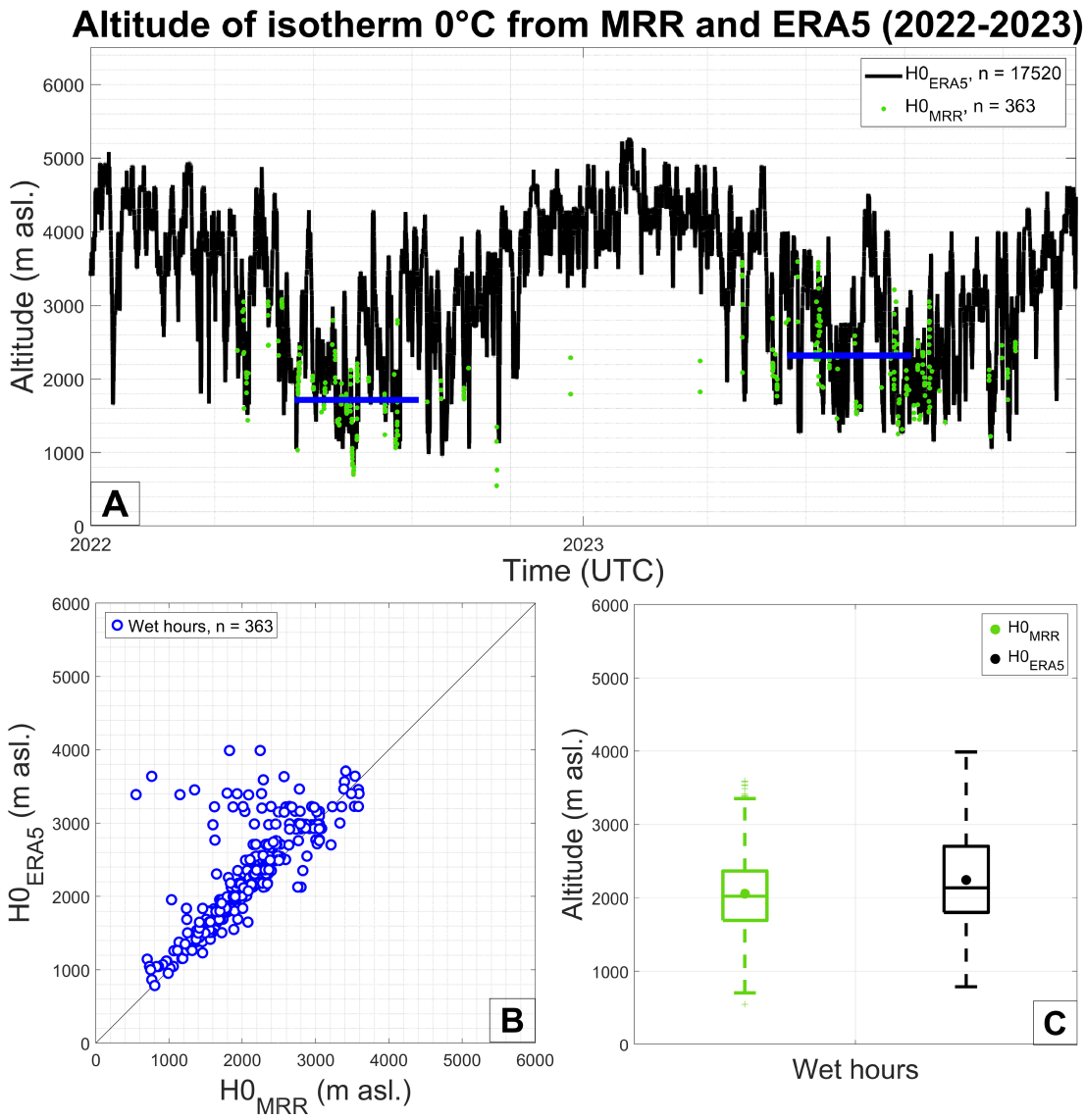

Figura 2.4.4: A) Time series of $H0_{ERA5}$ (in black) and $H0_{MRR}$ (in dark green); the blue horizontal lines correspond to the $H0_{MRR}$ averages of the 2022 and 2023 winter season. B) Scatter plot between $H0_{MRR}$ and $H0_{ERA5}$ for hours with precipitation (blue dots) recorded at Carriel Sur station. C) Same as B but in box plot.

2.5. Case studies

In this section, three precipitation events are analyzed. They were chosen to study the conditions accompanying the maximum and minimum recorded daily values of $H0_{MRR}$, considering as well to analyze $H0_{MRR}$ during the day with the highest precipitation.

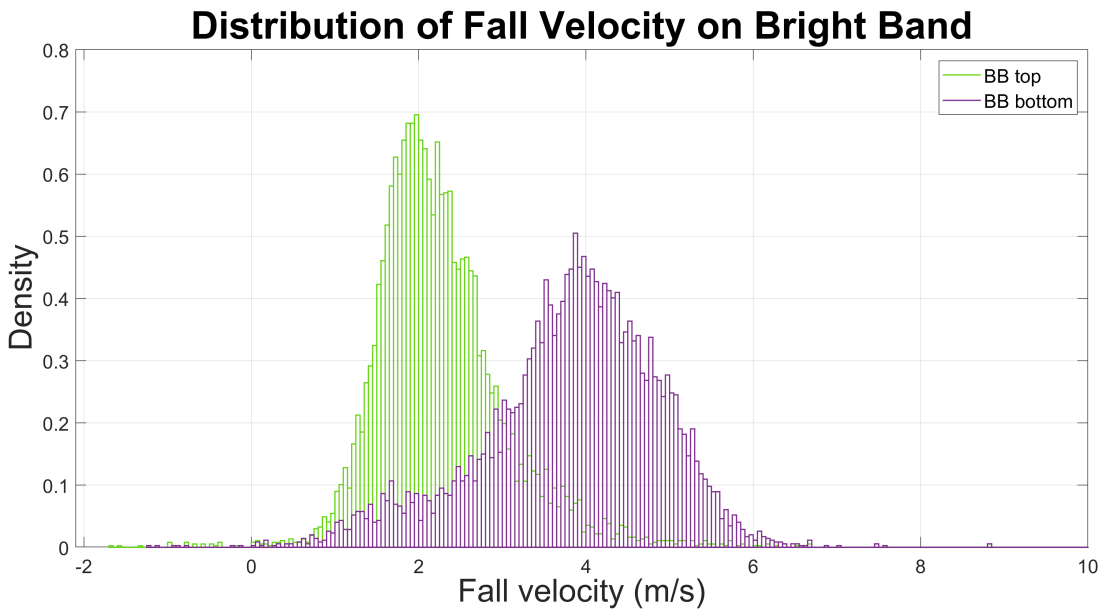

Figura 2.4.5: Distribution of hydrometeor fall velocity in the upper part of the bright band (green), i.e. H0, and in the lower part of the bright band (purple). The data are every 2 minutes.

The selection of these specific events is based on the aim to capture a range of atmospheric conditions, considering $H0_{MRR}$ from maximum and minimum, providing an understanding of how this variable behaves during the precipitation event, making a comparison in relation to the same variable obtained through reanalysis. In addition, focusing on the day with the highest precipitation allows a more detailed analysis of $H0_{MRR}$ under conditions of intense precipitation, further enriching the study.

1) Maximum daily $H0_{MRR}$: June 8, 2023

Precipitation began at 14 UTC on June 8, 2023 (Figure 2.5.1a, blue bar) and remained steady until 19 UTC, accumulating a total of 27.2 mm (considering 0.2 mm on the hours 04 and 08 UTC, then from 20 to 23 UTC), with maximum hourly precipitation of 9 mm at 17 UTC. The radar detects a reflectivity signal one hour before precipitation starts but is unable to identify the H0 due to an incomplete reflectivity profile (upper panel). The $H0_{MRR}$ was identified within three hours (15 to 17 UTC), being values above 3000 m asl, i.e., about 1000 m asl above the typical winter level. The mean $H0_{MRR}$ is ∼3200 m asl, the highest value in the period 2022-2023, while $H0_{ERA5}$ records >3400, i.e., ∼200 m lower

than the reanalysis. The MLT mean is ∼67 m; fall velocities close to H0 are ∼2.9 m/s on average, increasing to ∼3.3 m/s when crossing the bottom of the BB.

From the synoptic point of view, at 12 UTC the previous day (June 07; see Supplementary Figure A0.6a-b), the Pacific region shows that the large-scale circulation is dominated by anticyclonic conditions to the north of the country (∼20°S, ∼80°W) and a low pressure center is observed off the coasts of the study area, moisture transport and an area with high IVT is observed and has an inclined shape, the zonal flow dominates the mid-level circulation. For the day of interest June 8 at 12 UTC, the low-pressure system is positioned over the continent advancing towards Argentine territory (Figure 2.5.1d), leaving an accumulated precipitation of 27.2 mm during the day. It is shown in Figure 2.5.1c in an inclined band that reaches the Biobío coasts, with values close to 400 kg/ms.

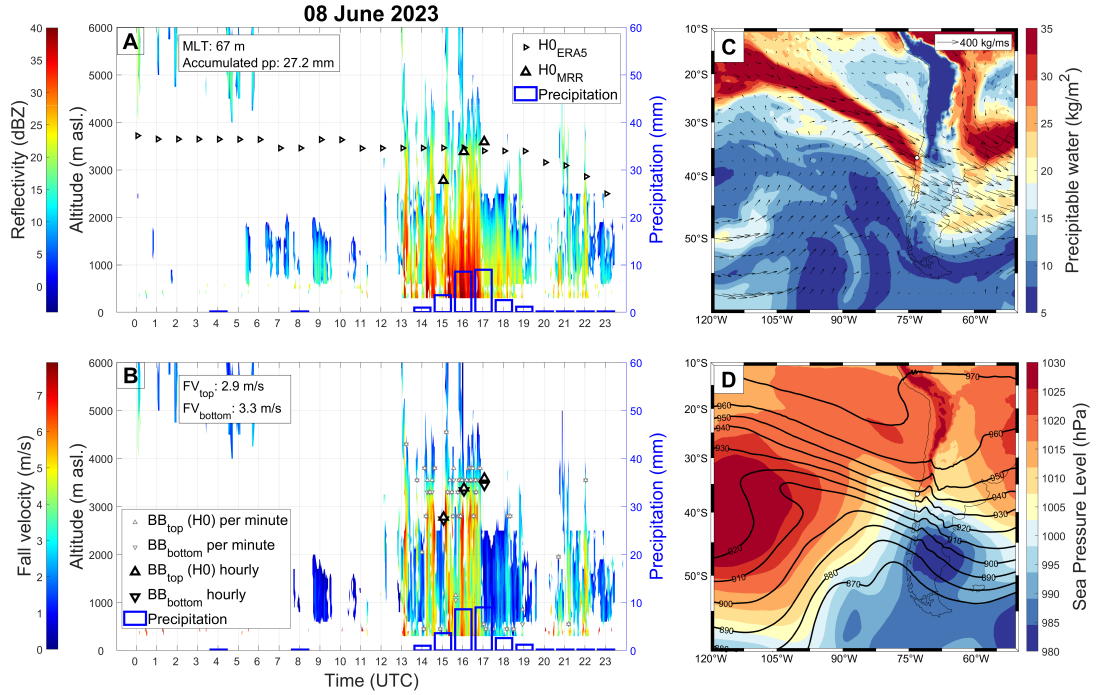

Figura 2.5.1: 08 June 2023. A) Same as Figure 4A. B) Same as 4B. C) Precipitable water (PW in colors in mm) and Integrated Water Vapor Transport (IVT vectors in kg/ms). D) Sea level pressure (shadows, hPa) and geopotential height at 300 hPa (contours, decameters). Variables in C and D are at 12 UTC and white dot in both figures indicates the position of the Biobío coastal zone.

2) Minimum daily H0: July 14, 2022

Throughout this day, the MRR intermittently detected reflectivity signals, and Carriel Sur station recorded a daily accumulated precipitation of 6.4 mm. Visually, the MRR detects reflectivity signals vertically over 2 km between 10 and 11 UTC without registering precipitation on the surface, it is observed signal 2 hours before surface precipitation (Figure 2.5.2a). The ML is visually observed at a height below 1 km, and the algorithm successfully identifies the hourly $H0_{MRR}$ of ∼700 m asl at 16 UTC. For that time $H0_{ERA5}$, ∼1100, i.e., ∼400 m over $H0_{MRR}$. For both datasets, this day resulted in the minimum daily mean. Considering daily means, the bottom of the BB was ∼ 163.2 m below the $H0_{MRR}$, and the mean fall velocity around the $H0_{MRR}$ was 1.9 m/s (Figure 2.5.2b).

Two days before the event, a zonal AR reached the study area, leaving an amount of 32.6 mm of accumulated precipitation and 14.4 mm the day before. To the south, a low-pressure center was observed off the coast of the southern zone (∼50°S), which left an amount of 15.4 mm of precipitation during July 13 (See Supplementary Figure A0.7a-b), moving northward until it reached the coast of the study area to the day 0 (Figure 2.5.2d), where it left an amount of 6.4 mm. Despite the small amount of precipitation left by the frontal system, the drop in temperature was noticeable, evidencing the low H0 values. No IVT values were observed for this day (Figure 2.5.2c).

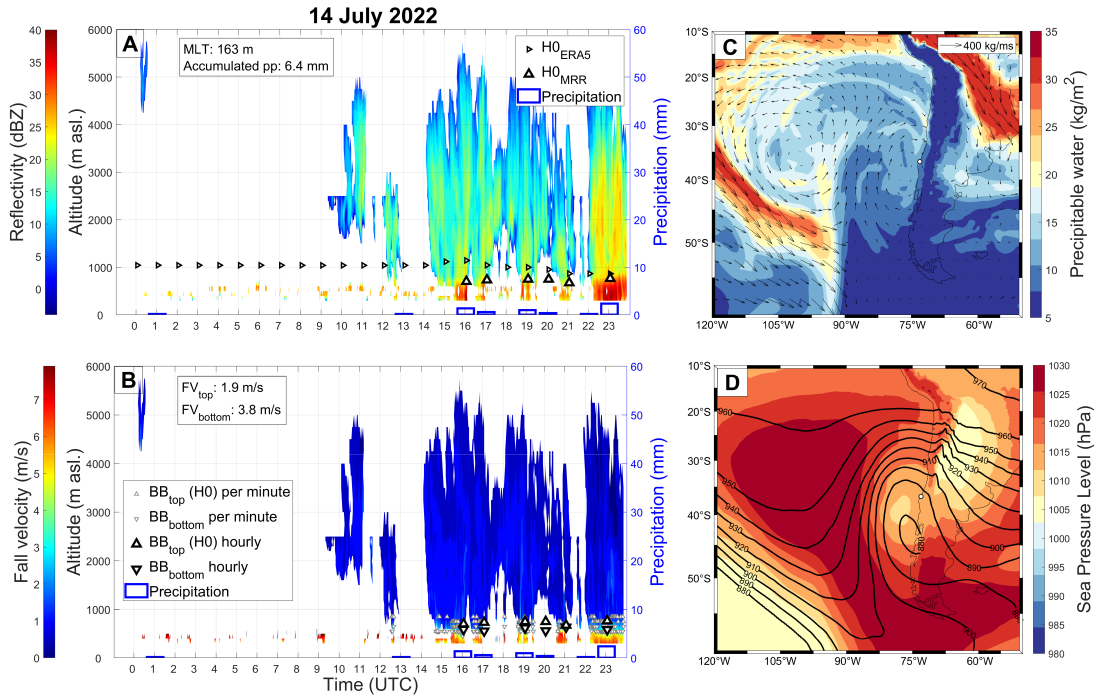

Figura 2.5.2: July 14, 2022. A) Same as Figure 4A. B) Same as 4B. C) Same as 8C. D) Same as 8D.

3) Maximum daily accumulated precipitation: June 04, 2022

On this day the highest daily precipitation in 2022 was recorded: 57.8 mm. Precipitation began at 01 UTC with a total of 0.4 mm, rising to 19.8 mm by 12 UTC and remaining constant throughout the day. At 17 UTC, an hourly amount of 12.4 mm was recorded (Figure 2.5.3a-b). It is worth noting that this day records the maximum accumulation of the period 2022-2023. BB is clearly observed due to persistent precipitation. The $H0_{MRR}$ reaches a daily mean value of ∼2100 m asl and remains constant throughout the storm (Figure 2.5.3a-b). The MLT shows a mean value of 221 m and the fall velocity across the $H0_{MRR}$ is 1.9 m/s.

The day with the highest accumulated precipitation began the previous day, leaving an amount of 41.8 mm where a low-pressure center (See Supplementary Figure A0.8a-b) is observed over the study area in the South Pacific, a deep trough is observed in the middle troposphere over another surface cyclone and water precipitable from lower latitudes in form of river. Then by June 4, the trough axis deepens, and observed a segregation in ∼32°S, ∼80°W (Figure 2.5.3d). Over the study area is left an amount of 57.8 mm of accumulated precipitation. A meridional AR is observed due to the high moisture content together with flow

from the north, obtaining a maximum magnitude of IVT in the study area of ∼ 200 kg/ms (Figure 2.5.3c).

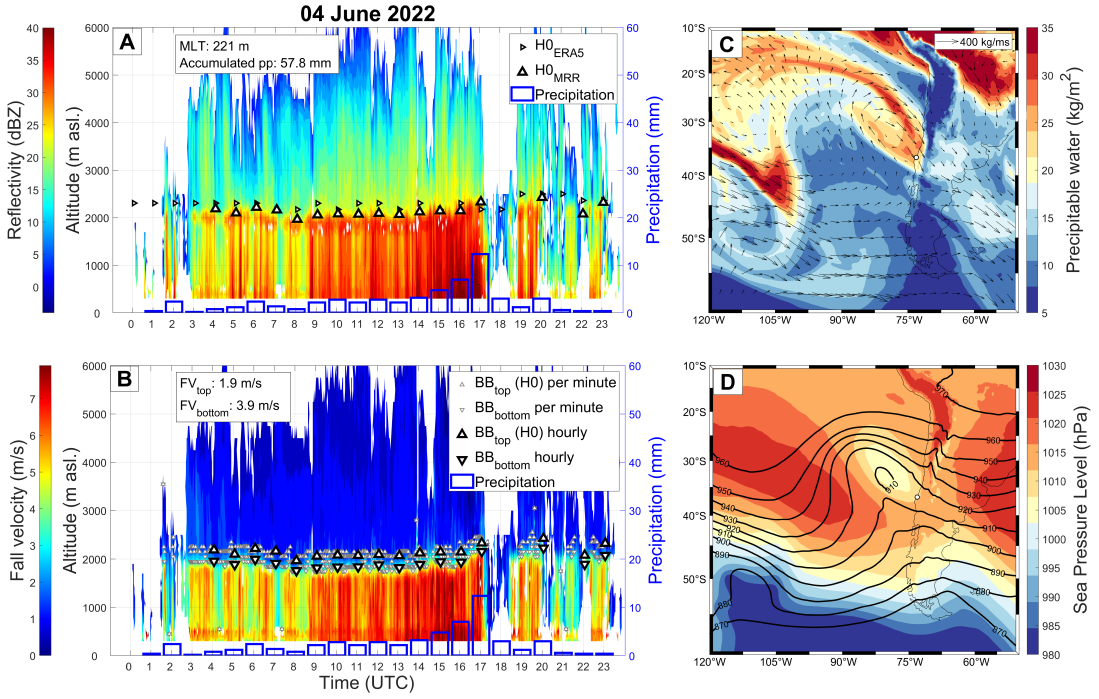

Figura 2.5.3: June 04, 2022. A) Same as Figure 4A. B) Same as 4B. C) Same as 8C. D) Same as 8D.

2.6. Conclusion

In this paper, the altitude of the 0ºC isotherm (H0) over the coast of the Biobío region in southern Chile was described using three data sources: observations, estimates and ERA5 reanalysis. During the period 2017-2019, $H0_{AMDAR}$ is compared with $H0_{ERA5}$, revealing a strong and positive correspondence, suggesting that ERA5 accurately described this variable in the study area and climatology was obtained and used as reference for H0 comparison in the following years. Hydrometeor reflectivity and fall velocity from a Micro Rain Radar are used to derive $H0_{MRR}$ for 2022-2023, and an algorithm originally developed by Schauwecker et al. (2017) for MRR data in Perú was developed to determine the Melting Layer Height, which is visually identifiable due to differences in the dielectric constants of snow and water, it was demonstrated that the top of this layer is considered as the top of this layer is considered as $H0_{MRR}$, with a mean of ∼2000 m asl.

Hydrometeors reach a mean fall velocity of 2.3 m/s across the $H0_{MRR}$.

The use of the MRR instrument offers several advantages. Regarding the scope of this study, firstly, hourly $H0_{MRR}$ values are obtained through an algorithm continuously and immediately (real-time) when precipitation occurs. The MRR captures precipitation signals through measurements of reflectivity and fall velocity. Within the constraints of the algorithm, we found that there are hours when surface precipitation is recorded but the MRR instrument fails to pick up that signal, in some cases it is because it is very weak since most of those amounts are usually around 0.1 millimeter of precipitation and in other cases the fact that the Carriel Sur station is located 6 km from the MRR is considered, being a factor to consider since it is possible that it precipitates in one place and not in the other (considering the same hour). Moreover, compared to the reanalysis, lower $H0_{MRR}$ values are observed in some hours, all these data agree that the radar variables do now show data above 3000 m asl, and the algorithm interprets the negative gradient with the values available, biasing the H0 value obtained at lower altitudes. Despite this, when precipitation occurs and the algorithm is applied, it can identify and successfully quantify the altitude level of the H0 at the minute level. In order to be able to use these values at the hourly level, the data completeness criterion is applied, and some hours are discarded. This fact implies that continuous precipitation for 1 hour is necessary for the estimation of the $H0_{MRR}$ at hour level. Through the radar images and due to the differences in the dielectric constants of snow and water, the H0 is visually identifiable, so the proposed method provides a numerical estimate to the visualization of the melt layer. Another important advantage is that the algorithm also provides information about the bright band, information that was not available before in the region. We obtain a mean ML value of ∼170 m, which is within the maximum range of 300 m of thickness between the top and bottom of the BB.

The cases analyzed here are specific events which we observed the evolution of the H0, when this has a high value (associated to warm state), the thickness of the melting layer is lower in relation of the case in which the event is associated with cold conditions (the H0 has an average below 1000 m asl) and the melting layer occurs within a greater thickness. Therefore, when crossing H0 the snowflakes must travel a greater distance in cold conditions to complete the melting and arrive as water droplets to the surface over the coast of the Biobío Region.

As part of future work, we suggest the application of the algorithm to more recent radar data for the creation of an $H0_{MRR}$ database over the Biobío coastal zone. This study contributes by starting with the 2022 and 2023 MRR data. Ideally, it is expected to complete this database with data from 2024 and continue with the process as long as there is MRR data. On the other hand, the MRR can provide other types of information, such as precipitation patterns, that have been characterized in numerous studies worldwide. This work contributes to a first attempt to describe the variability of H0 and opens the possibility of implementing the described algorithm in further studies. Also, H0 is an important variable in high mountains, so it is natural to think that these applications would be beneficial in the interior of the Biobío region, close to the Andes Mountain.

Capítulo 3

Conclusión

En este trabajo se describió la altitud de la isoterma 0^{o}C (H0) sobre la zona costera de la región del Biobío, Chile, utilizando tres fuentes de datos: observaciones, estimaciones y reanálisis ERA5. Durante el período 2017-2019, $H0_{AMDAR}$ se compara con $H0_{ERA5}$, revelando una fuerte y positiva correspondencia, lo que sugiere que ERA5 describe con precisión esta variable en el área de estudio y se obtiene la climatología, la cual se utilizó como referencia para la comparación de H0 en los años siguientes. La reflectividad de los hidrometeoros y la velocidad de caída del Micro Rain Radar se utilizan para derivar $H0_{MRR}$ para los años 2022-2023, y se utiliza un algoritmo originalmente desarrollado por Schauwecker et al. (2017) en Perú para determinar la altitud de capa de derretimiento, que es visualmente identificable debido a las diferencias en las constantes dieléctricas de la nieve y el agua, se demostró que la parte superior de esta capa se considera como $H0_{MRR}$, con una media de ∼2000 m snm. Los hidrometeoros alcanzan una velocidad media de caída de 2.3 m/s a través de la $H0_{MRR}$.

El uso del instrumento MRR ofrece varias ventajas. En relación con el ámbito de este estudio, en primer lugar, los valores horarios del $H0_{MRR}$ se obtienen mediante un algoritmo de forma continua e inmediata (en tiempo real) cuando se producen precipitaciones. El MRR capta las señales de precipitación mediante las variables de reflectividad y velocidad de caída. Dentro de las limitaciones del algoritmo, comprobamos que hay horas en las que se registran precipitaciones en superficie pero el instrumento MRR no capta esa señal, en algunos casos es porque es muy débil ya que la mayoría de esas cantidades suelen estar bajo el 0.1 mm de

precipitación y en otros casos se considera el hecho de que la estación Carriel Sur se encuentra a 6 km del MRR, siendo un factor a considerar puesto que es posible que precipite en un lugar y en el otro no (considerando la misma hora). Además, en comparación con el reanálisis, se observan valores de $H0_{MRR}$ más bajos en algunas horas, todos estos datos coinciden en que las variables radar no muestran datos por encima de los 3000 m snm, y el algoritmo interpreta el gradiente negativo con los valores disponibles, sesgando el valor de H0 obtenido a menor altitud. A pesar de ello, cuando se producen precipitaciones y se aplica el algoritmo, éste puede identificar y cuantificar con éxito el nivel de H0 considerando la resolución cada 2 minutos. Para poder utilizar estos valores a nivel horario, se aplica el criterio de completitud de los datos y se descartan algunas horas.

Los casos aquí analizados son eventos puntuales en los que observamos la evolución de la H0, cuando ésta tiene un valor alto (asociado condiciones cálidas), el espesor de la capa de fusión es menor en relación al caso en que el evento está asociado a condiciones frías (la H0 tiene un promedio inferior a 1000 m snm) y la capa de fusión se produce dentro de un espesor mayor. Por lo tanto, al cruzar el H0 los copos de nieve deben recorrer una mayor distancia en condiciones frías para completar el derretimiento y llegar como gotas de agua a la superficie sobre la costa de la Región del Biobío.

Como parte del trabajo futuro, se sugiere la aplicación del algoritmo a datos de radar más recientes para la creación de una base de datos $H0_{MRR}$ sobre la zona costera del Biobío. Este estudio contribuye comenzando con los datos MRR de los años 2022 y 2023. Idealmente, se espera completar esta base de datos con datos de 2024 y continuar con el proceso mientras existan datos MRR. Por otro lado, el MRR puede proporcionar otro tipo de información, como los patrones de precipitación, que han sido caracterizados en numerosos estudios a nivel mundial. Este trabajo contribuye a un primer intento de describir la variabilidad de H0 y abre la posibilidad de aplicar el algoritmo descrito en estudios posteriores. Además, H0 es una variable importante en alta montaña, por lo que es natural pensar que estas aplicaciones serían beneficiosas en el interior de la región del Biobío, en zonas cercanas a la Cordillera de los Andes.

Bibliografía

Aceituno, P., Boisier, J. P., Garreaud, R., Rondanelli, R., and Rutllant, J. A. (2021). Climate and weather in Chile. *Water resources of Chile*, pages 7–29.

AMS (2021). American Meteorological Society Glossary 2nd ed. Boston. http://amsglossary.allenpress.com/glossary/brows. Accessed on March 4, 2024.

Austin, P. M. and Bemis, A. C. (1950). A quantitative study of the "bright band" in radar precipitation echoes. *Journal of Atmospheric Sciences*, 7(2):145–151.

Barrett, B. S., Garreaud, R., and Falvey, M. (2009). Effect of the Andes Cordillera on precipitation from a midlatitude cold front. *Monthly Weather Review*, 137(9):3092–3109.

Battan, L. (1973). Radar observation of the atmosphere.

Benarroch, A., Siles, G. A., Riera, J. M., and Pérez-Peña, S. (2020). Heights of the 0° c isotherm and the bright band in madrid: Comparison and variability. In *2020 14th European Conference on Antennas and Propagation (EuCAP)*, pages 1–5. IEEE.

Boodoo, S., Hudak, D., Donaldson, N., and Leduc, M. (2010). Application of dual-polarization radar melting-layer detection algorithm. *Journal of Applied Meteorology and Climatology*, 49(8):1779–1793.

Brast, M. and Markmann, P. (2020). Detecting the melting layer with a micro rain radar using a neural network approach. *Atmospheric Measurement Techniques*, 13(12):6645–6656.

C3S (2017). ERA5: Fifth Generation of ECMWF Atmospheric Reanalyses of the Global Climate. U. K. Copernic. Clim. Change Serv. Clim. Data Store (CDS). https://cds.climate.copernicus.eu/cdsapp#!/home.. Accessed on 15 February 2023.

Endries, J. L., Perry, L. B., Yuter, S. E., Seimon, A., Andrade-Flores, M., Winkelmann, R., Quispe, N., Rado, M., Montoya, N., Velarde, F., et al. (2018). Radar-observed characteristics of precipitation in the tropical high Andes of southern Peru and Bolivia. *Journal of Applied Meteorology and Climatology*, 57(7):1441–1458.

Fabry, F. and Zawadzki, I. (1995). Long-term radar observations of the melting

layer of precipitation and their interpretation. *Journal of the atmospheric sciences*, 52(7):838–851.

Garcia-Benadi, A., Bech, J., Udina, M., Campistron, B., and Paci, A. (2022). Multiple characteristics of precipitation inferred from wind profiler radar Doppler spectra. *Remote Sensing*, 14(19):5023.

García-Lee, N., Bravo, C., Gónzalez-Reyes, Á., and Mardones, P. (2024). Spatial and temporal variability of the freezing level in Patagonia's atmosphere. *Weather and Climate Dynamics*, 5(3):1137–1151.

Garreaud, R. D. (2009). The Andes climate and weather. *Advances in geosciences*, 22:3–11.

Garreaud, R. D. (2013). Warm winter storms in Central Chile. *Journal of Hydrometeorology*, 14(5):1515–1534.

Garreaud, R. D., Jacques-Coper, M., Marín, J. C., and Narváez, D. A. (2024). Atmospheric Rivers in South-Central Chile: Zonal and Tilted Events. *Atmosphere*, 15(4):406.

Ghada, W., Casellas, E., Herbinger, J., Garcia-Benadí, A., Bothmann, L., Estrella, N., Bech, J., and Menzel, A. (2022). Stratiform and convective rain classification using machine learning models and micro rain radar. *Remote Sensing*, 14(18):4563.

Glickman, T. and Walter, Z. (2000). Glossary of Meteorology. Amer. Meteor. Soc., 855 pp.

Grantham, T. E., Figueroa, R., and Prat, N. (2013). Water management in mediterranean river basins: a comparison of management frameworks, physical impacts, and ecological responses. *Hydrobiologia*, 719:451–482.

Harris, G. N., Bowman, K. P., and Shin, D.-B. (2000). Comparison of freezing-level altitudes from the NCEP reanalysis with TRMM precipitation radar brightband data. *Journal of climate*, 13(23):4137–4148.

Hersbach, H., Bell, B., Berrisford, P., Hirahara, S., Horányi, A., Muñoz-Sabater, J., Nicolas, J., Peubey, C., Radu, R., Schepers, D., et al. (2020). The ERA5 global reanalysis. *Quarterly Journal of the Royal Meteorological Society*, 146(730):1999–2049.

Hooper, J. and Kippax, A. (1950). The bright band—A phenomenon associated with radar echoes from falling rain. *Quarterly Journal of the Royal Meteorological Society*, 76(328):125–132.

Ibañez, M., Gironás, J., Oberli, C., Chadwick, C., and Garreaud, R. D. (2021). Daily and seasonal variation of the surface temperature lapse rate and 0°c isotherm height in the western subtropical andes. *International Journal of Climatology*, 41:E980–E999.

Leary, C. A. and Houze, R. A. (1979). Melting and evaporation of hydrometeors in precipitation from the anvil clouds of deep tropical convection. *Journal of the Atmospheric Sciences*, 36(4):669–679.

Lundquist, J. D., Neiman, P. J., Martner, B., White, A. B., Gottas, D. J., and Ralph, F. M. (2008). Rain versus snow in the Sierra Nevada, California: Comparing Doppler profiling radar and surface observations of melting level. *Journal of Hydrometeorology*, 9(2):194–211.

Mardones, P. and Garreaud, R. D. (2020). Future changes in the free tropospheric freezing level and rain–snow limit: The case of central Chile. *Atmosphere*, 11(11):1259.

Marks, D., Winstral, A., Reba, M., Pomeroy, J., and Kumar, M. (2013). An evaluation of methods for determining during-storm precipitation phase and the rain/snow transition elevation at the surface in a mountain basin. *Advances in Water Resources*, 55:98–110.

Massmann, A. K., Minder, J. R., Garreaud, R. D., Kingsmill, D. E., Valenzuela, R. A., Montecinos, A., Fults, S. L., and Snider, J. R. (2017). The Chilean Coastal Orographic Precipitation Experiment: Observing the influence of microphysical rain regimes on coastal orographic precipitation. *Journal of Hydrometeorology*, 18(10):2723–2743.

Matrosov, S. Y. (2008). Assessment of radar signal attenuation caused by the melting hydrometeor layer. *IEEE Transactions on Geoscience and Remote Sensing*, 46(4):1039–1047.

Mehta, S., Mehta, S. K., Singh, S., Mitra, A., Ghosh, S. K., and Raha, S. (2020). Characteristics of the Z–R Relationships Observed Using Micro Rain Radar (MRR-2) over Darjeeling (27.05 N, 88.26 E): A Complex Terrain Region in the Eastern Himalayas. *Pure and Applied Geophysics*, 177:4521–4534.

METEK, G. (2008). MRR-2 Micro Rain RADAR User Manual. 01.2008 Version 4.12 / 4.15. https://www.inscc.utah.edu/~u0546592/CFOG/4DHIRAJ/mrr-manual.pdf. Retrieved on November 4, 2020.

Minder, J. R. and Kingsmill, D. E. (2013). Mesoscale variations of the atmospheric snow line over the northern Sierra Nevada: Multiyear statistics, case study, and mechanisms. *Journal of the Atmospheric Sciences*, 70(3):916–938.

Muñoz, R. C., Whiteman, C. D., Garreaud, R. D., Rutllant, J. A., and Hidalgo, J. (2022). Using commercial aircraft meteorological data to assess the heat budget of the convective boundary layer over the Santiago Valley in Central Chile. *Boundary-Layer Meteorology*, 183(2):295–319.

Pechan, P. M., Obster, F., Marchioro, L., and Bohle, H. (2023). Climate change impact on fruit farm operations in Chile and Tunisia. *agriRxiv*, (2023):20230025166.

Perry, L. B., Seimon, A., Andrade-Flores, M. F., Endries, J. L., Yuter, S. E., Velarde, F., Arias, S., Bonshoms, M., Burton, E. J., Winkelmann, I. R., et al. (2018). Characteristics of precipitating storms in glacierized tropical Andean Cordilleras of Peru and Bolivia. In *Mountains: Physical, Human-Environmental, and Sociocultural Dynamics*, pages 74–86. Routledge.

Peters, G., Fischer, B., and Andersson, T. (2002). Rain observations with a vertically looking Micro Rain Radar (MRR). *Boreal environment research*, 7(4):353–362.

Pfaff, T., Engelbrecht, A., and Seidel, J. (2014). Detection of the bright band with a vertically pointing k-bandradar.

Ramadhan, R., Marzuki, M., Vonnisa, M., Harmadi, H., Hashiguchi, H., and Shimomai, T. (2021). Comparison of Bright Band Radar from GPM and MRR Observation in West Sumatera. *Jurnal Penelitian Fisika dan Aplikasinya (JPFA)*, 11(1):50–62.

Sánchez-Diezma, R., Zawadzki, I., and Sempere-Torres, D. (2000). Identification of the bright band through the analysis of volumetric radar data. *Journal of Geophysical Research: Atmospheres*, 105(D2):2225–2236.

Sarricolea-Espinoza, P., Herrera Ossandón, M., and Meseguer Ruiz, Ó. (2017). Climatic regionalisation of continental Chile.

Schauwecker, S., Palma, G., MacDonell, S., Ayala, Á., and Viale, M. (2022). The snowline and 0°c isotherm altitudes during precipitation events in the dry subtropical Chilean Andes as seen by citizen science, surface stations, and ERA5 reanalysis data. *Frontiers in Earth Science*, 10:875795.

Schauwecker, S., Rohrer, M., Huggel, C., Endries, J., Montoya, N., Neukom, R., Perry, B., Salzmann, N., Schwarb, M., and Suarez, W. (2017). The freezing level in the tropical Andes, Peru: An indicator for present and future glacier extents. *Journal of Geophysical Research: Atmospheres*, 122(10):5172–5189.

Seidel, J., Trachte, K., Orellana-Alvear, J., Figueroa, R., Célleri, R., Bendix, J., Fernandez, C., and Huggel, C. (2019). Precipitation characteristics at two locations in the tropical Andes by means of vertically pointing micro-rain radar observations. *Remote Sensing*, 11(24):2985.

Shulgina, T., Gershunov, A., Hatchett, B. J., Guirguis, K., Subramanian, A. C., Margulis, S. A., Fang, Y., Cayan, D. R., Pierce, D. W., Dettinger, M., et al. (2023). Observed and projected changes in snow accumulation and snowline in California's snowy mountains. *Climate Dynamics*, 61(9):4809–4824.

Smith, B. L. and Blaes, J. L. (2015). Examination of a Winter Storm Using a Micro Rain Radar and AMDAR Aircraft Soundings. *Journal of Operational Meteorology*.

Stickland, J. and Grooters, A. (2005). The global AMDAR programme. *measurement*, 100:0–001.

Valenzuela, R. A. and Garreaud, R. D. (2019). Extreme daily rainfall in central-southern Chile and its relationship with low-level horizontal water vapor fluxes. *Journal of Hydrometeorology*, 20(9):1829–1850.

Viale, M. and Garreaud, R. (2015). Orographic effects of the subtropical and extratropical Andes on upwind precipitating clouds. *Journal of Geophysical Research: Atmospheres*, 120(10):4962–4974.

Viale, M., Valenzuela, R., Garreaud, R. D., and Ralph, F. M. (2018). Impacts of atmospheric rivers on precipitation in southern South America. *Journal of Hydrometeorology*, 19(10):1671–1687.

White, A. B., Gottas, D. J., Strem, E. T., Ralph, F. M., and Neiman, P. J. (2002). An automated brightband height detection algorithm for use with Doppler radar spectral moments. *Journal of Atmospheric and Oceanic Technology*, 19(5):687–697.

Wilks, D. S. (2011). *Statistical methods in the atmospheric sciences*, volume 100. Academic press.

Yevenes, M. A., Figueroa, R., and Parra, O. (2018). Seasonal drought effects on the water quality of the Biobío River, Central Chile. *Environmental science and pollution research*, 25:13844–13856.

Apéndice A

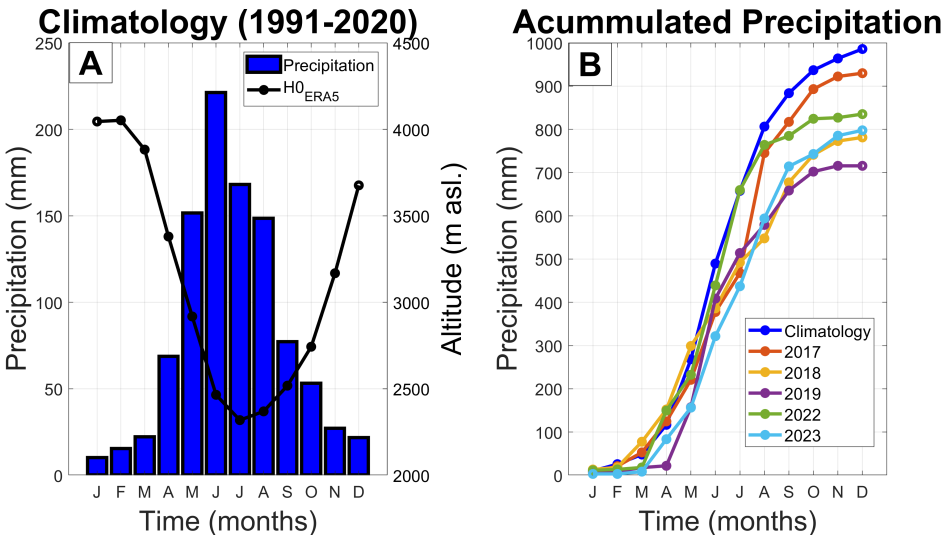

Figura A0.1: A) Climatology of precipitation and $H0_{ERA5}$ (1991-2020). B) Comparison of accumulated climatology of precipitation and study years.

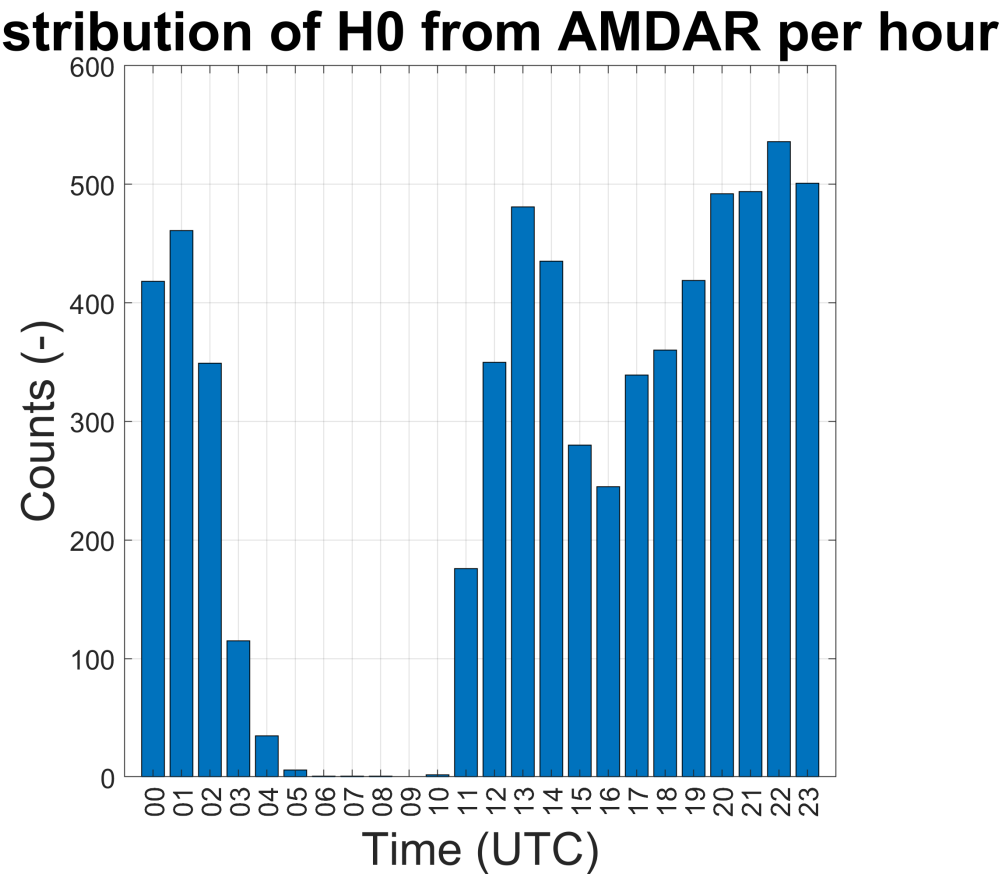

Figura A0.2: Distribution of available $H0_{AMDAR}$ values between 00 and 23 UTC.

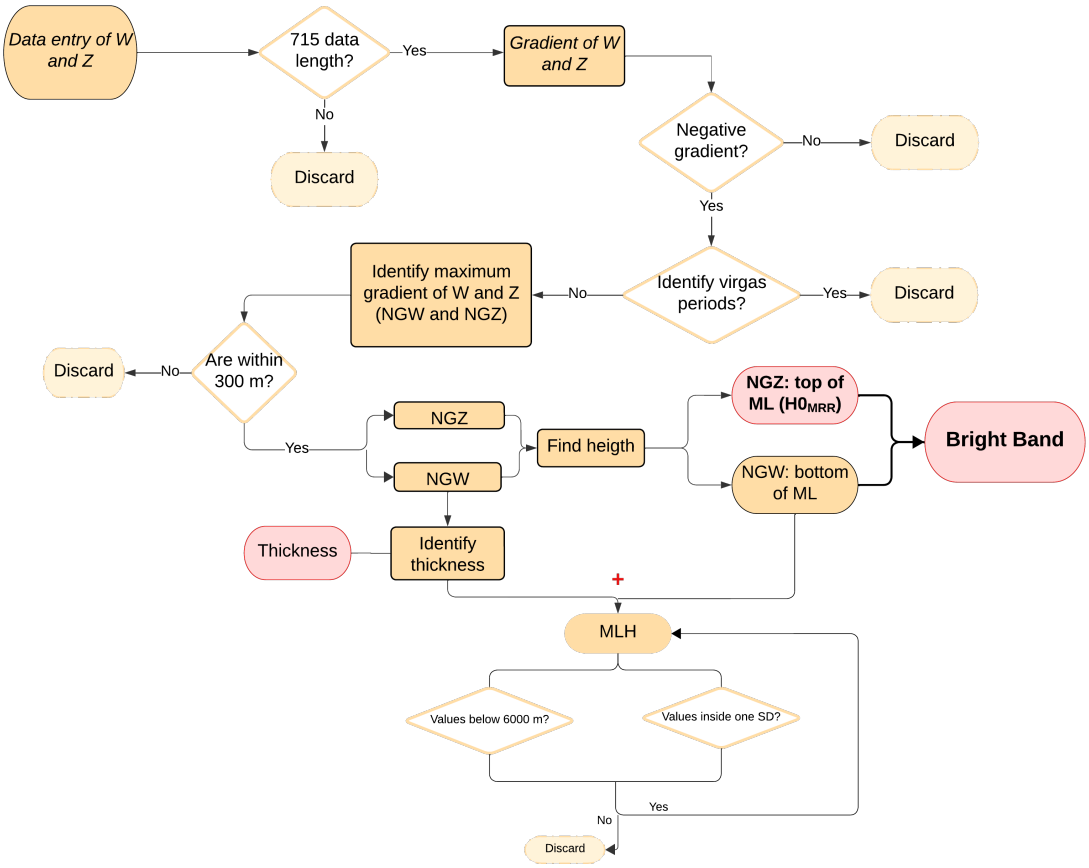

Figura A0.3: flowchart for the algorithm methodology

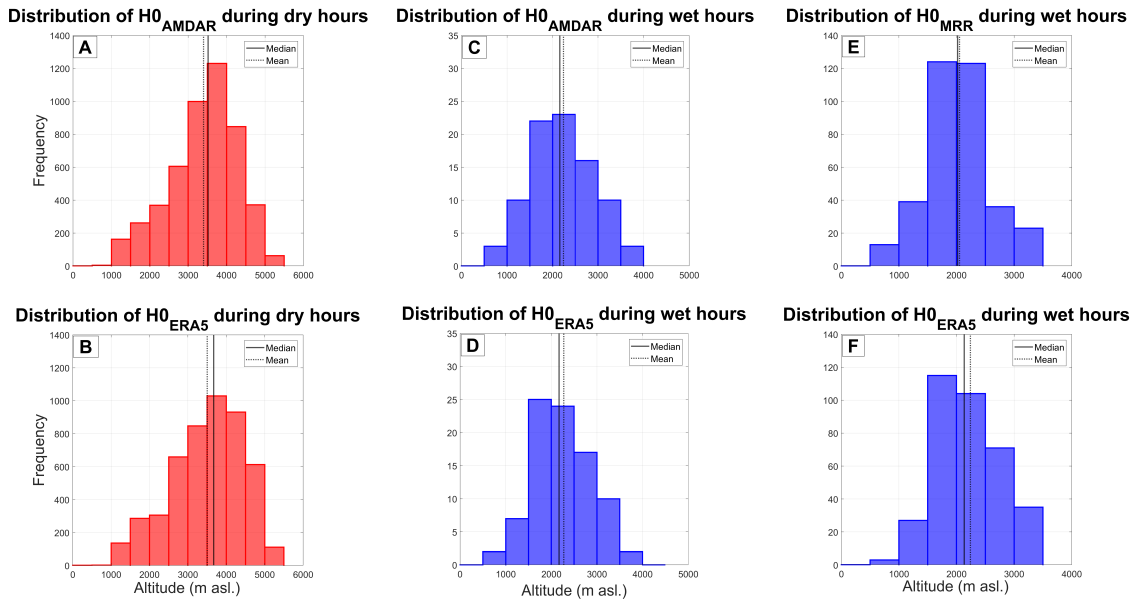

Figura A0.4: Period: 2017 - 2019. A) Frequency distribution of $H0_{AMDAR}$ data for dry hours. B) Same as A but for $H0_{ERA5}$ data. C) Frequency distribution of $H0_{AMDAR}$ data for wet hours. D) Same as C but for $H0_{ERA5}$ data. E) Frequency distribution of $H0_{MRR}$ data for wet hours. F) Same as E but for $H0_{ERA5}$ data.

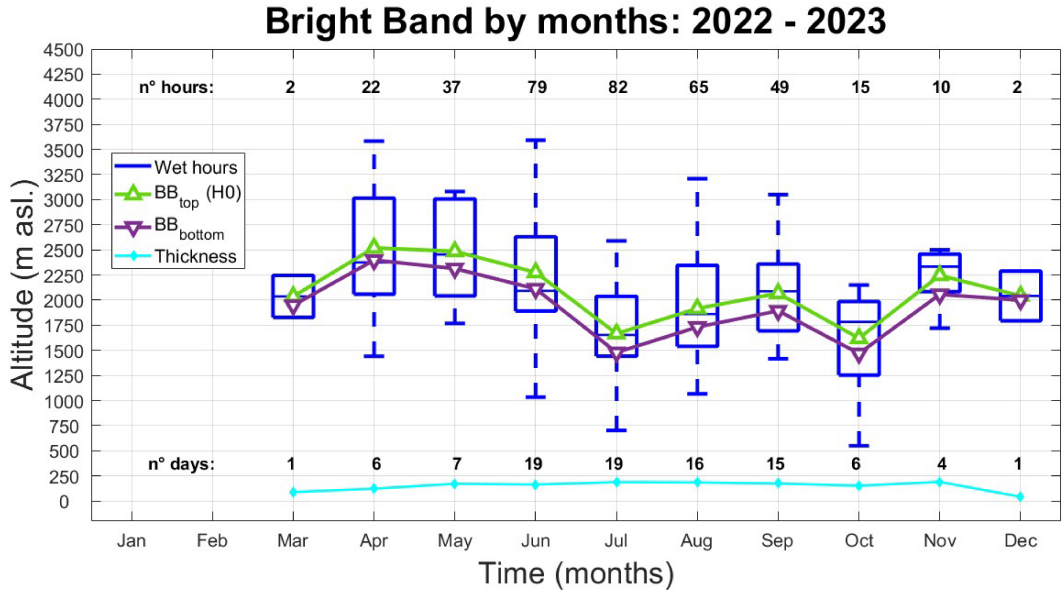

Figura A0.5: Bright Band by months for 2022 and 2023 from MRR, represented by the green triangles which are the top part ($H0_{MRR}$), the purple triangles are the bottom part, furthermore, in light blue color is the difference between both parts of the bright band, i.e. the thickness.

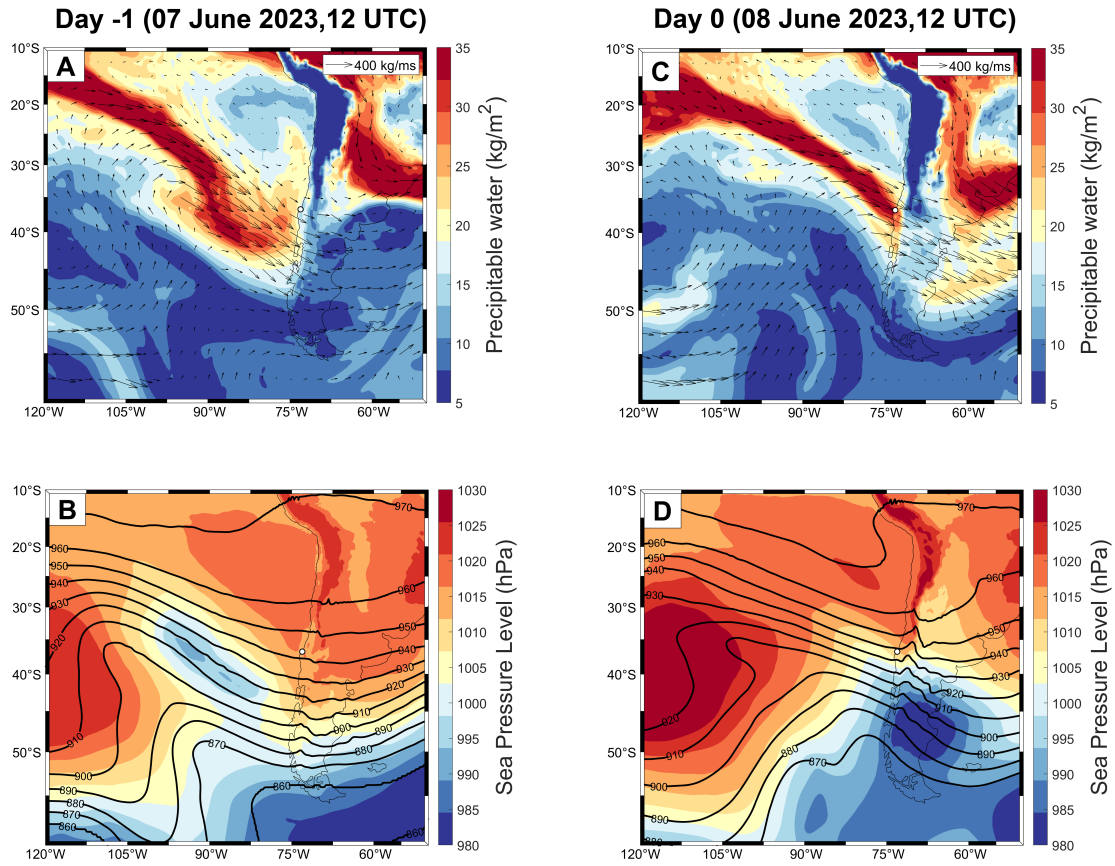

Figura A0.6: Day 07 June 2023: A) Precipitable water (PW in colors in mm) and Integrated Water Vapor Transport (IVT vectors in kg/ms). B) Sea level pressure (shadows, hPa) and geopotential height at 300 hPa (contours, decameters). Day 08 June 2023: C) As A. D) As B. White dot in both figures indicates the position of the Biobío coastal zone.

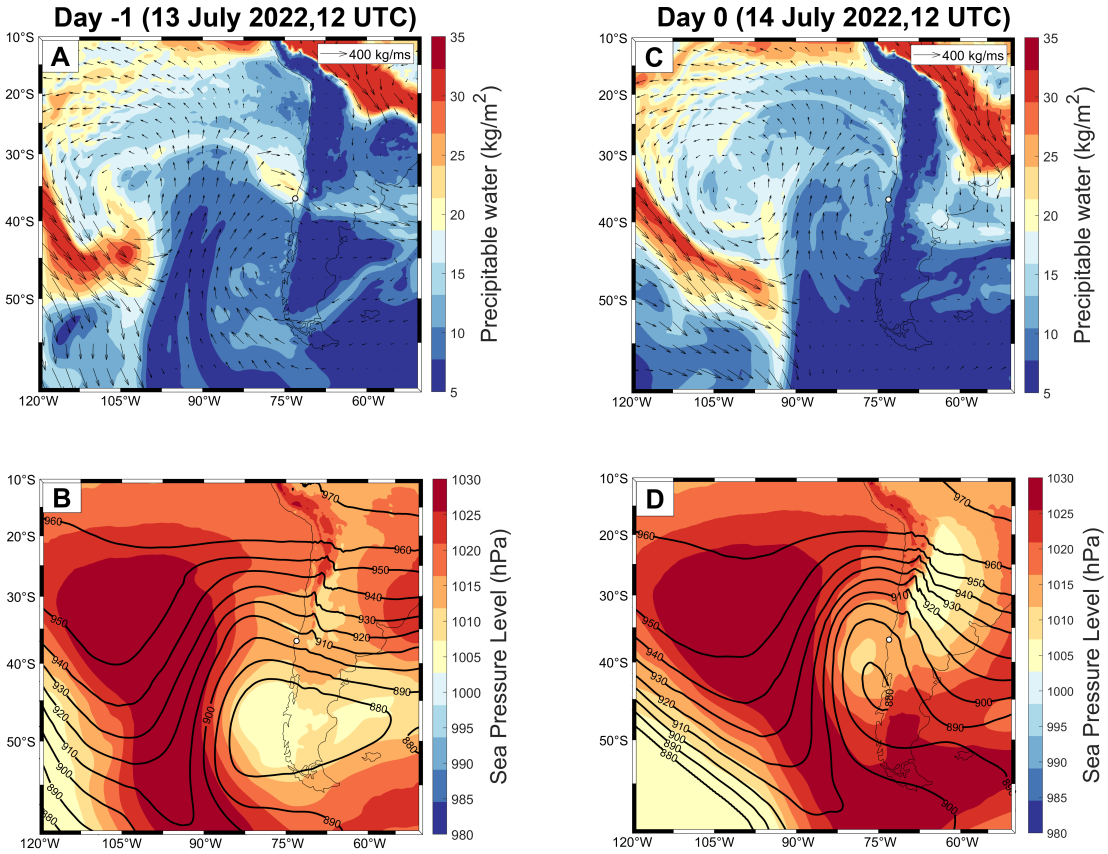

Figura A0.7: Day 13 july 2022: A) Precipitable water (PW in colors in mm) and Integrated Water Vapor Transport (IVT vectors in kg/ms). B) Sea level pressure (shadows, hPa) and geopotential height at 300 hPa (contours, decameters). Day 14 july 2022: C) As A. D) As B. White dot in both figures indicates the position of the Biobío coastal zone.

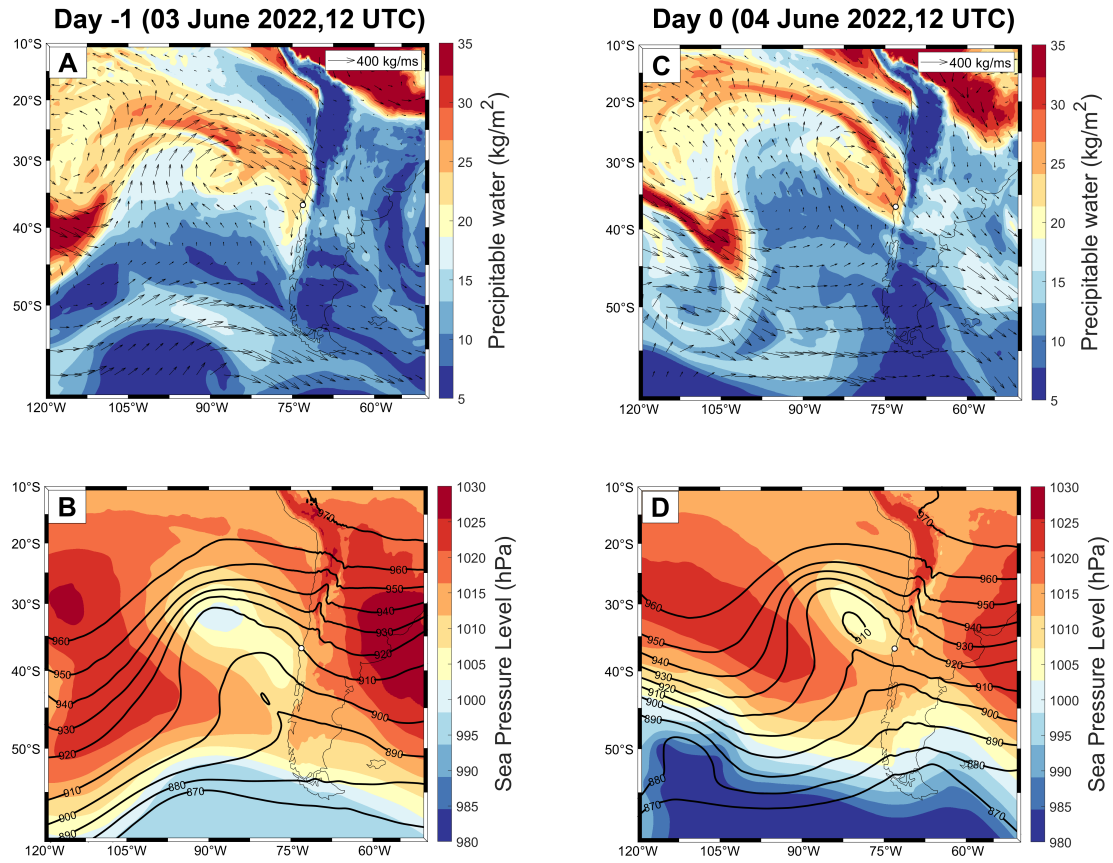

Figura A0.8: Day 03 June 2022: A) Precipitable water (PW in colors in mm) and Integrated Water Vapor Transport (IVT vectors in kg/ms). B) Sea level pressure (shadows, hPa) and geopotential height at 300 hPa (contours, decameters). Day 04 June 2022: C) As A. D) As B. White dot in both figures indicates the position of the Biobío coastal zone.